# Synthesis, Pharmacological Assessment, and Molecular Modeling of Acetylcholinesterase/Butyrylcholinesterase Inhibitors: Effect against Amyloid-β-Induced Neurotoxicity

**ARTICLE** *in* ACS CHEMICAL NEUROSCIENCE · FEBRUARY 2013

Impact Factor: 4.36 · DOI: 10.1021/cn300178k · Source: PubMed

ACS Chemical Neuroscience

Research Article

pubs.acs.org/chemneuro

# Synthesis, Pharmacological Assessment, and Molecular Modeling of Acetylcholinesterase/Butyrylcholinesterase Inhibitors: Effect against Amyloid-$\beta$-Induced Neurotoxicity

Daniel Silva,[†,‡] Mourad Chioua,[‡] Abdelouahid Samadi,[‡] Paula Agostinho,*[,§,∥] Pedro Garção,[§,∥] Rocío Lajarín-Cuesta,[⊥] Cristobal de los Ríos,[⊥] Isabel Iriepa,[#] Ignacio Moraleda,[#] Laura Gonzalez-Lafuente,[⊥] Eduarda Mendes,[†] Concepción Pérez,[▽] María Isabel Rodríguez-Franco,[▽] José Marco-Contelles,*[,‡] and M. Carmo Carreiras*[,†]

[†]Research Institute for Medicines and Pharmaceutical Sciences (iMed.UL), Faculty of Pharmacy, University of Lisbon, Av. Prof. Gama Pinto, 1649-003 Lisbon, Portugal

[‡]Laboratorio de Química Médica (IQOG, CSIC), C/Juan de la Cierva 3, 28006-Madrid, Spain

[§]Center for Neuroscience and Cell Biology, University of Coimbra, 3004-517 Coimbra, Portugal

[∥]Faculty of Medicine, University of Coimbra, 3004-504 Coimbra, Portugal

[⊥]Instituto Teófilo Hernando, Fundación de Investigación Biomédica, Hospital Universitario de la Princesa, C/Diego de Léon, 62, 28006-Madrid, Spain

[#]Departamento de Química Orgánica. Universidad de Alcalá, Ctra. Madrid-Barcelona, Km. 33,6, 28871, Alcalá de Henares, Madrid, Spain

[▽]Instituto de Química Médica, Consejo Superior de Investigaciones Científicas (IQM-CSIC), C/Juan de la Cierva 3, 28006-Madrid, Spain

Supporting Information

**ABSTRACT:** The synthesis, molecular modeling, and pharmacological analysis of phenoxyalkylamino-4-phenylnicotinates (**2**−**7**), phenoxyalkoxybenzylidenemalononitriles (**12**, **13**), pyridonepezils (**14**−**18**), and quinolinodonepezils (**19**−**21**) are described. Pyridonepezils **15**−**18** were found to be selective and moderately potent regarding the inhibition of hAChE, whereas quinolinodonepezils **19**−**21** were found to be poor inhibitors of hAChE. The most potent and selective hAChE inhibitor was ethyl 6-(4-(1-benzylpiperidin-4-yl)butylamino)-5-cyano-2-methyl-4-phenylnicotinate (**18**) [$IC_{50}$ (hAChE) = 0.25 ± 0.02 $\mu$M]. Pyridonepezils **15**−**18** and quinolinodonepezils **20**−**21** are more potent selective inhibitors of *Ee*AChE than hAChE. The most potent and selective *Ee*AChE inhibitor was ethyl 6-(2-(1-benzylpiperidin-4-yl)ethylamino)-5-cyano-2-methyl-4-phenylnicotinate (**16**) [$IC_{50}$ (*Ee*AChE) = 0.0167 ± 0.0002 $\mu$M], which exhibits the same inhibitory potency as donepezil against hAChE. Compounds **2**, **7**, **13**, **17**, **18**, **35**, and **36** significantly prevented the decrease in cell viability caused by A$\beta_{1-42}$. All compounds were effective in preventing the enhancement of AChE activity induced by A$\beta_{1-42}$. Compounds **2**−**7** caused a significant reduction whereas pyridonepezils **17** and **18**, and compound **16** also showed some activity. The pyrazolo[3,4-*b*]quinolines **36** and **38** also prevented the upregulation of AChE induced by A$\beta_{1-42}$. Compounds **2**, **7**, **12**, **13**, **17**, **18**, and **36** may act as antagonists of voltage sensitive calcium channels, since they significantly prevented the $Ca^{2+}$ influx evoked by KCl depolarization. Docking studies show that compounds **16** and **18** adopted different orientations and conformations inside the active-site gorges of hAChE and hBuChE. The structural and energetic features of the **16**-AChE and **18**-AChE complexes compared to the **16**-BuChE and **18**-BuChE complexes account for a higher affinity of the ligand toward AChE. The present data indicate that compounds **2**, **7**, **17**, **18**, and **36** may represent attractive multipotent molecules for the potential treatment of Alzheimer's disease.

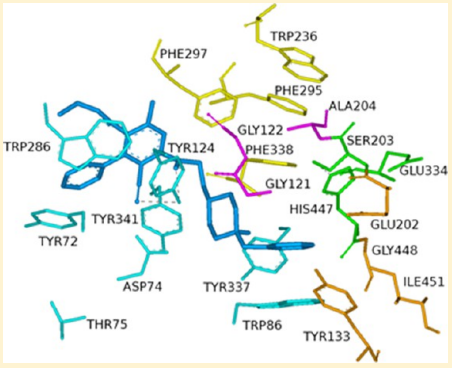


**KEYWORDS:** *Pyridonepezils, quinolinodonepezils, AChE/BuChE inhibitors, Aβ peptide, neuroprotection, $Ca^{2+}$ dyshomeostasis, Alzheimer's disease*

Alzheimer's disease (AD) is the most prevalent neurodegenerative disorder.[1] AD is characterized by the gradual development of forgetfulness, progressing to disturbances in language, disorientation, and mutism. The symptomatic course

**Received:** October 11, 2012
**Accepted:** January 19, 2013
**Published:** February 4, 2013

  

**Chart 1. Structure of Donepezil, Molecules 1−13, Pyridonepezils 14−18, and Quinolinodonepezils 19−21**

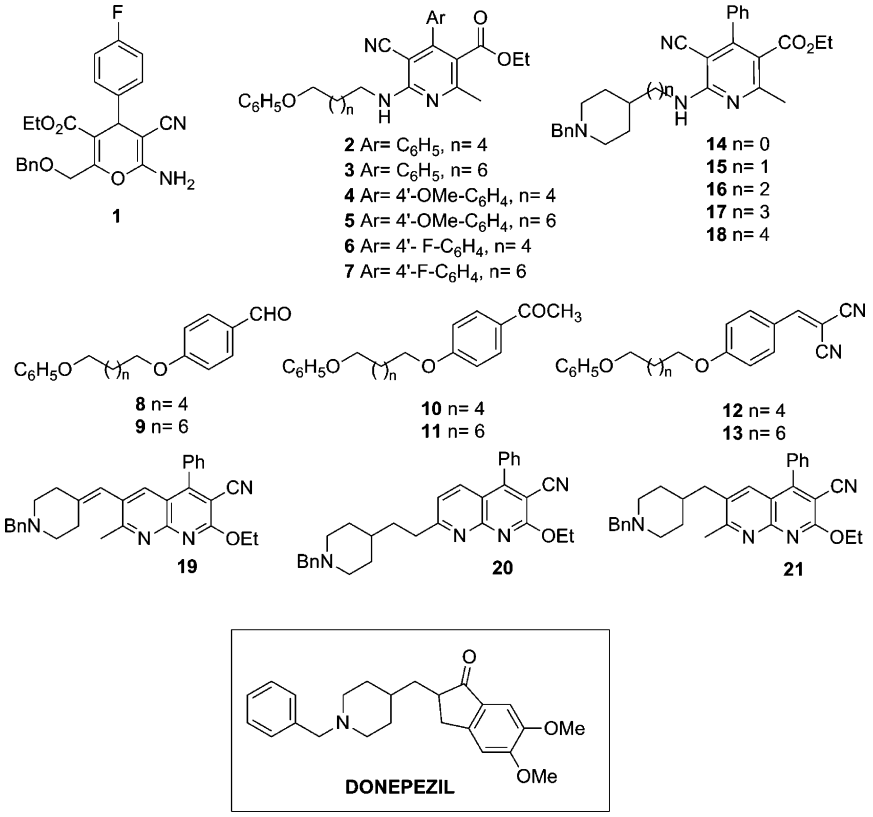


of disease is generally 5 or more years of stepwise decline in memory and attention span, and has been described.[2] Classical pathological hallmarks are extracellular senile plaques, consisting principally of amyloid-$\beta$ (A$\beta$), and intracellular neurofibrillary tangles, which are composed of phosphorylated tau protein. Moreover, the basal nucleus of Meynert undergoes profound neuron loss, and the neocortex exhibits a loss of cholinergic fibers and receptors and a decrease of both choline acetyltransferase and acetylcholinesterase (AChE) enzyme activity.[2,3]

Since the symptoms of AD were associated with an altered cholinergic function, research has focused on the basal forebrain cholinergic system.[3] As a result, the cholinergic hypothesis was developed, which postulated that a loss of cholinergic function in the central nervous system contributed significantly to cognitive decline associated with advanced age and AD.[4] Thus, drugs capable of inhibiting AChE might potentiate central cholinergic function, therefore improving cognition and perhaps even some of the behavioral problems experienced by AD patients.[5]

AChE inhibitors (AChEIs) may inhibit AChE via a competitive mechanism, by interacting with the catalytic center (CC) of the enzyme, via a noncompetitive mechanism, by binding with the peripheral anionic site (PAS), or via both mechanisms, by exerting a dual binding AChE inhibition.[5] For a while the treatment with AChEIs was reported to produce only symptomatic improvement, having no effect in the course of the disease.[6] However, other studies indicated that AChE interacts with A$\beta$ by an hydrophobic environment close to the PAS, thus promoting A$\beta$ fibril formation.[7,8] Moreover, AChE-A$\beta$ complexes increase A$\beta$-dependent neurotoxicity.[9] These reports arose a new interest in AChEIs. Thus, early investigations demonstrated the ability of cholinesterase inhibitors (ChEIs) to enhance the release of nonamyloidogenic soluble derivatives of amyloid precursor protein (APP) in vitro and in vivo, and possibly to slow down formation of amyloidogenic compounds in the brain.[10] The increase of soluble APP (APPs) was also consistent with AChE inhibition.[11] Numerous clinical trials have demonstrated the safety and efficacy of ChEIs in the treatment of AD. Besides, there is growing evidence from preclinical studies indicating that these agents can attenuate neuronal damage and death from cytotoxic insults and, therefore, might affect AD pathogenesis.[12]

Considering the noncholinergic aspects of AChE related to its PAS[7−9] in associating with A$\beta$, an attractive target for the design of new antidementia drugs emerged. Peripheral or dual site inhibitors of AChE may simultaneously alleviate the cognitive deficit in AD patients and prevent the assembly of A$\beta$, which will delay the neurodegenerative process.[13] This strategy was pursued by several medicinal chemists who have been developing new compounds with dual AChE inhibitory activity,[14−17] based on well-known AChEIs such as tacrine,[18] rivastigmine,[19] donepezil,[20] and galanthamine.[21]

For tacrine, several homodimeric tacrine-based AChEIs were synthesized. Their increased inhibitory potency was assigned to the simultaneous binding of the units to the active and peripheral anionic sites of AChE.[22,23] One of these novel compounds, heptylene-linked bis-tacrine, was found to be 150-fold more active against rat AChE than tacrine and 250-fold more selective for AChE than for BuChE.[15] Similarly, donepezil-tacrine,[24] melatonin-tacrine,[25] tacrine-ferulic acid hybrids,[26] indanone and aurone derivatives,[27] or multitarget-


dx.doi.org/10.1021/cn300178k | ACS Chem. Neurosci. 2013, 4, 547−565

directed coumarin derivatives[28] have been investigated with success.

$Ca^{2+}$ is one of the most important intracellular messengers in the brain, being essential for neuronal development, synaptic transmission, and plasticity in neurons by influencing the cytoskeleton and associated proteins.[29,30] Calcium signals can be used to control many processes in the cell. The calcium hypothesis of brain aging and neurodegenerative disorders such as AD states that long-term, slightly elevated cytosolic $Ca^{2+}$ levels ($[Ca^{2+}]_i$) and/or disturbances in $Ca^{2+}$ homeostasis represent the cellular mechanisms underlying neuronal aging.[31] Under resting conditions, cytosolic $Ca^{2+}$ is maintained at low nanomolar concentrations by a collection of pumps, buffers, and transport mechanisms. $Ca^{2+}$ entry into the cytosol is rigorously regulated and originates from one of two major sources: the extracellular fluid via entry across the plasma membrane (through receptor-, voltage-, and store-operated channels and $Ca^{2+}$ exchangers) and intracellular stores such as the endoplasmic reticulum (ER) and mitochondria.[32] A$\beta$ interaction with the plasma membrane results in elevated $[Ca^{2+}]_i$ and increased vulnerability of neurons to excitotoxicity. Oligomeric forms of A$\beta_{42}$ cause $Ca^{2+}$-mediated toxicity in cultured cells. Degenerative changes occur in neurites associated with A$\beta$ deposits in APP mutant mice, suggesting the involvement of $Ca^{2+}$-mediated A$\beta$ neurotoxicity in vivo. In addition to increasing the production of A$\beta$, amyloidogenic processing of APP can perturb neuronal $Ca^{2+}$ homeostasis by decreasing the production of a secreted form of APP that activates $K^+$ channels, and by generating an APP intracellular domain that affects ER $Ca^{2+}$ release by regulating the expression of genes involved in $Ca^{2+}$ homeostasis.[33] Studies of patients, and animal and cell culture models, have provided a wealth of data supporting the involvement of alterations in $Ca^{2+}$ regulation in the pathogenesis of stroke and chronic neurodegenerative disorders. Analyses of brain tissues from patients with a neurodegenerative disease have revealed evidence that alterations in cellular $Ca^{2+}$ homeostasis contribute to the neurodegenerative process.[34] Thus, different multitarget-directed drug families have been developed, taking into account the key role of $Ca^{2+}$ in neurodegenerative diseases.[35]

In the context of our continued interest in the development of new multipotent drugs for the treatment of AD,[35,36] we have recently started a project targeted to the design and biological analysis of dual AChEIs endowed with additional properties. Due to the prevalent selection of donepezil as a partner in high efficient and potent dual AChEIs,[37] and the well-known anticholinesterase and antiamnesic activities reported for aminopyridine derivatives from this[38] and other laboratories,[39] in this work we describe the synthesis and biological assessment of pyridine-donepezil (pyridonepezils) and dual AChEIs **14**–**18**, as well as the quinolyl-donepezil (quinolinodonepezils) derivatives **19**–**21** (Chart 1). From these compounds, ethyl 6-((2-(1-benzylpiperidin-4-yl)ethyl)amino)-5-cyano-2-methyl-4-phenylnicotinate (**16**) (Chart 1) has emerged as a dual, and quite selective hAChE as well as *Ee*AChE inhibitor, showing moderate activity for the inhibition of hBuChE.

## RESULTS AND DISCUSSION

**Chemistry.** In the first exploratory experiments, ethyl 6-amino-2-((benzyloxy)methyl)-5-cyano-4-(4-fluorophenyl)-4*H*-pyran-3-carboxylate (**1**), *N*-alkyl (ethyl 6-amino-5-cyano-2-methyl-4-arylnicotinates) (**2**–**7**), *O*-alkyl [4-hydroxybenzaldehyde (**8**,**9**), and 1-(4-hydroxyphenyl)ethanone (**10**, **11**), 2-(4-hydroxybenzylidene)malononitrile (**12**, **13**)[40] (Chart 1) bearing linear methylene spacers of 6 or 8 carbon atoms connecting the pyridine nucleus with a phenyl ring have been synthesized (see the Supporting Information) and evaluated showing in general no inhibition (Table 3) for both ChEs.[40] These results moved us to install the *N*-benzylpiperidine motif present in donepezil (Chart 1), connected with suitable spacers to different heterocyclic ring systems, such as polysubstituted pyridines or [1,8]-naphthyridines.

The syntheses of pyridonepezils **14**–**17** (Chart 1) have been carried out by *N*-alkylation of readily available ethyl 6-chloro-5-cyano-2-methyl-4-phenylnicotinate (**22**)[41] with commercial 4-amino-1-benzylpiperidine (**23**), (1-benzylpiperidin-4-yl)-methanamine (**24**),[42] 2-(1-benzylpiperidin-4-yl)ethanamine (**25**),[42] and 3-(1-benzylpiperidin-4-yl)propan-1-amine (**26**)[43] in high yield (Scheme 1).

**Scheme 1. Synthesis of Pyridonepezils 14–18**

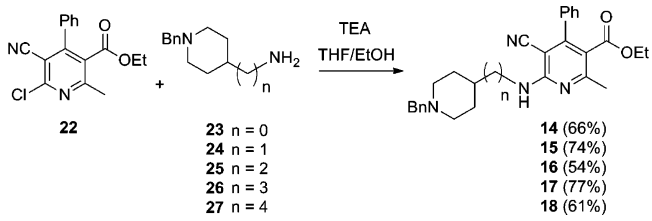


For the preparation of pyridonepezil **18**, we have synthesized 4-(1-benzylpiperidin-4-yl)butan-1-amine (**27**) here, for the first time, as shown in Scheme 2, starting from alcohol **28**.[44] After reaction with DPPA, DBU, and sodium azide in DMF, azide **29** was isolated, whose reduction with triphenylphosphine/water/THF afforded the envisaged amine. Next, the reaction of amine **27** with pyridine **22** gave, as usual, the expected compound **18** in good yield (Scheme 1).

All the new compounds gave satisfactory analytical and spectroscopic data in good agreement with the expected structures (see Methods).

Quinolinodonepezil **19** (Chart 1) has been prepared by Friedländer reaction[45,46] of 6-amino-2-ethoxy-5-formyl-4-phenylnicotinonitrile (**30**)[47] and (*E*)-4-(1-benzylpiperidin-4-yl)-but-3-en-2-one (**32**) (Scheme 3), prepared from commercially available 1-benzylpiperidine-4-carbaldehyde (**31**) by standard Wittig–Horner–Wadsworth–Emmons reaction (Scheme 4). The structure of compound **19** has been assigned after inspection of its analytical and spectroscopic data (see Methods). Particularly diagnostic was the presence of two singlets for one proton each at $\delta$ 7.52 and 6.19, for H-5 and H-4″ {C(6)–C(*H*)=C[$(CH_2)_2(CH_2)_2$]NBn}, respectively. A weak NOE effect between these two protons but a clear and stronger NOE effect between protons at H5 and C(7)$CH_3$ at $\delta$ 2.70 suggest that a major rotamer in the equilibrium should be the one depicted for compound **19** (Scheme 3). Thus, only compound **19** was isolated, in moderate yield, and no traces of the other Friedländer-possible product **34** (Scheme 3) was observed.

In Scheme 3, we show a possible mechanism in order to explain the formation of compound **19**. Two possible routes have been considered. Via route (A), the base reacts with the acidic $\gamma$-H giving a delocalized allylic carbanion, which by intermolecular reaction of the carbanion at the allylic carbon (C$\alpha$) with the aldehyde group should afford the aldol product, which after elimination of water would provide a mixture of *E*/


dx.doi.org/10.1021/cn300178k | ACS Chem. Neurosci. 2013, 4, 547–565

**Scheme 2. Synthesis of 4-(1-Benzylpiperidin-4-yl)butan-1-amine (27)**

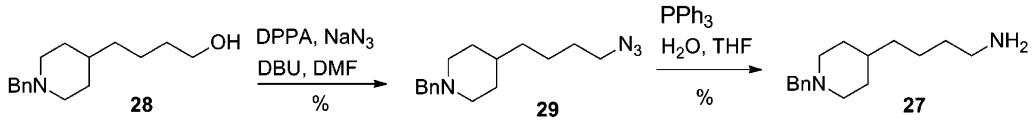


**Scheme 3. Reaction Conditions [a. 10% KOH/EtOH (49%)] and Proposed Mechanism for the Formation of Quinolinodonepezil 19**

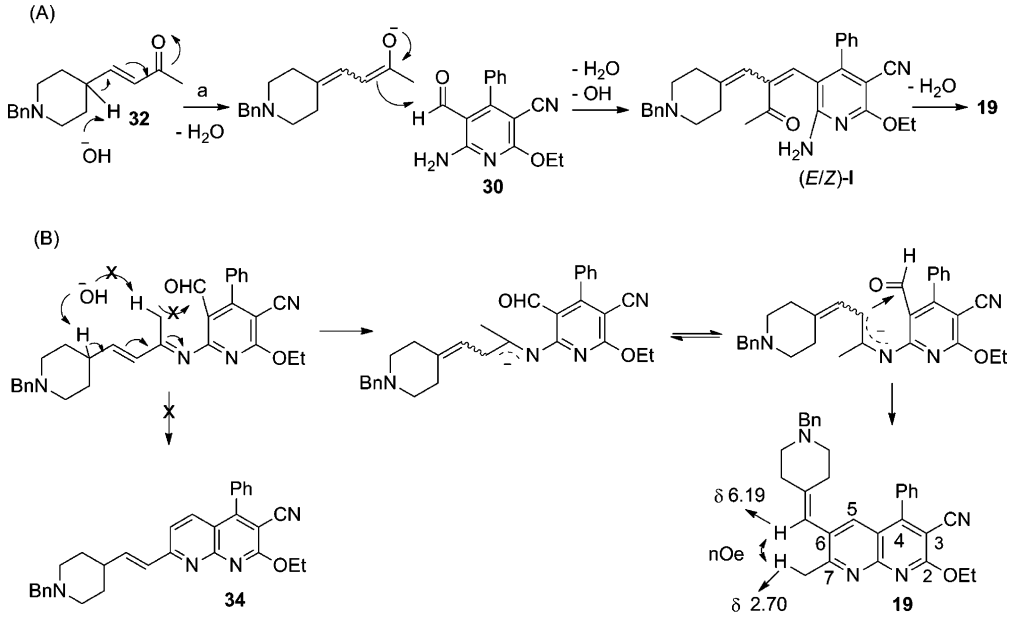


**Scheme 4. Synthesis of Ketones 32 and 33**

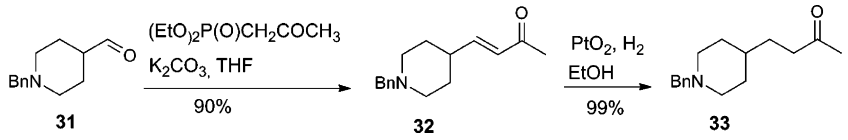


**Scheme 5**[a]

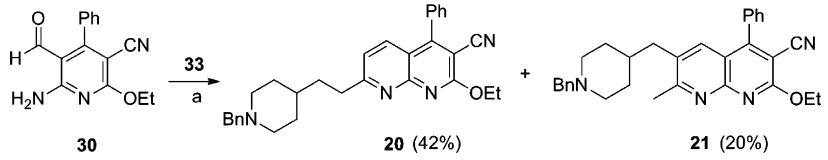


[a]Reaction conditions: (a) Pyrrolidine, $CH_2Cl_2$/MeOH.

*Z*-**I** intermediates. Obviously, only isomer *Z*-**I** could react with the amino group to give compound **19**, a fact that could explain the modest yield obtained. However, note that we were unable to detect the *E*-**I** isomer or any other secondary product. We cannot rule out the alternative via (B) (Scheme 3), where the formation of the imine/enamine mixture precedes the intramolecular cyclization leading to compound **19**. In this scenario, deprotonation of the methyl group ($CH_3CO-$) leading finally to compound **34** (Scheme 3) should be clearly disfavored. Finally, it has to be highlighted that, to the best of our knowledge, this is the first example of Friedländer reaction[45,46] of a *o*-aminobenzaldehyde with a 4-alkyl substituted butan-2-one.

Similarly, a mixture of compounds **20** and **21** (Chart 1) was obtained by Friedländer reaction[45,46] of compound **30** with ketone **33** (Scheme 5) using pyrrolidine as catalyst.[48] The structures of the resulting quinolinodonepezils **20** and **21** were determined by $^1$H and $^{13}$C NMR spectroscopy and elemental analysis. The appearance of signals at $\delta$ 7.85 (d, $J$ = 8.4 Hz, 1H) and 7.22 (d, 1H, $J$ = 8.4 Hz, CH), corresponding to H5 and H6, in the $^1$H NMR spectrum of compound **20**, as well as two singlets at $\delta$ 7.53 and 2.76, integrating for one and three protons, and corresponding to H5 and C(7)$CH_3$, respectively, in the $^1$H NMR spectrum of compound **21**, clearly support the structure of the Friedländer products. The formation of major reaction product **20**, as the result of a preferred intramolecular cyclization through the methyl versus the methylene group, leading to major C-7 susbtituted [1,8]naphthyridine, is also in good agreement with previous results reported in the literature from similar reagents using the same catalyst.[49]


dx.doi.org/10.1021/cn300178k | *ACS Chem. Neurosci.* 2013, 4, 547−565

**Chart 2. Structures of Pyrazole Derivatives 35−37**[50]

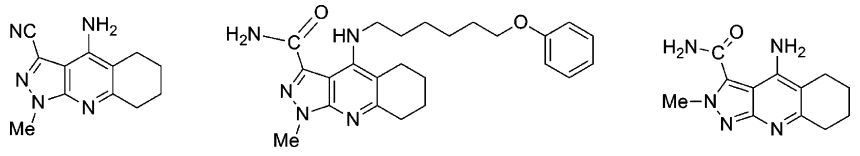

35 36 37

The syntheses of pyrazolo[3,4-*b*]quinolines **35**−**37** (Chart 2) and their inhibitory activity against *Ee*AChE/eqBuChE were previously described.[50] The neuroprotective activity of compounds **35**−**37** against A$\beta$-induced cytotoxicity as well as their effect in intracellular $Ca^{2+}$ homeostasis dysregulation triggered by A$\beta$ are reported in this work.

**Pharmacology.** *Inhibition of EeAChE and eqBuChE by Compounds 14−21.* Pyridonepezils **14**−**18** and quinolinodonepezils **20,21** were evaluated as inhibitors of AChE from *Electrophorus electricus* (*Ee*AChE) and BuChE from horse serum (eqBuChE) (Table 1), according to the protocol of Ellman et al.[51] The inhibitory activities of the hybrids were compared to those determined for the parent compound, donepezil. Compound **14** was not soluble, so its biological assessment was not possible. Comparing this data with the results shown in Table 2, we can see that pyridonepezils **15**−**18** and quinolinodonepezils **20,21** are more potent inhibitors of *Ee*AChE than hAChE ($IC_{50}$ values ranging from 0.0167 to 2.7 $\mu$M, Table 1). In general, they are also more potent to eqBuChE than to hBuChE, as $IC_{50}$ values range from 0.31 to 10 $\mu$M (Table 1).

**Table 1. Inhibition of *Ee*AChE and eqBuChE by Pyridonepezils (14−18) and Quinolinodonepezils (20,21)**[a]

| Compound | Structure | $IC_{50}$ AChE (μM) | $IC_{50}$ BuChE (μM) |
|---|---|---|---|
| Donepezil | 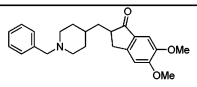 | 0.0134 ± 0.0009 | 0.84 ± 0.05 |
| 14 | 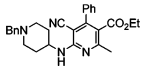 | --[b] | --[b] |
| 15 | 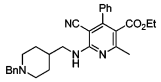 | 0.79 ± 0.06 | 1.50 ± 0.08 |
| 16 | 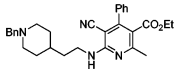 | 0.0167 ± 0.0007 | 0.88 ± 0.08 |
| 17 | 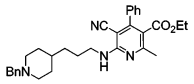 | 0.019 ± 0.002 | 0.31 ± 0.05 |
| 18 | 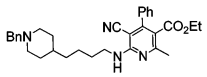 | 0.030 ± 0.004 | 0.380 ± 0.018 |
| 19 | 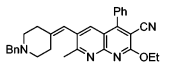 | nd[c] | nd[c] |
| 20 | 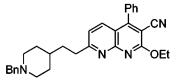 | 0.10 ± 0.01 | 10 ± 1.7 |
| 21 | 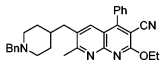 | 2.7 ± 0.5 | >10 |

[a]Data are expressed as the mean ± SEM of at least three different experiments in quadruplicate. [b]Nonsoluble. [c]nd: Not determined.

**Table 2. Inhibition of hAChE/hBuChE by Pyridonepezils (14−18) and Quinolinodonepezils (19−21)**[a]

| Compound | Structure | $IC_{50}$ hAChE (μM) | $IC_{50}$ hBuChE (μM) |
|---|---|---|---|
| Donepezil | 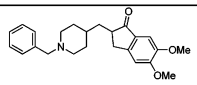 | 0.016 ± 0.001[b] | 8.2 ± 0.2[c] |
| 14 | 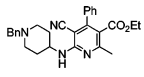 | --[d] | --[d] |
| 15 | 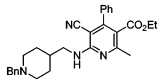 | 4.57 ± 1.50 | >10 |
| 16 | 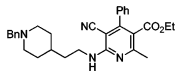 | 0.31 ± 0.04 | 4.00 ± 0.50 |
| 17 | 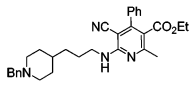 | 0.32 ± 0.037 | 8.59±0.60 |
| 18 | 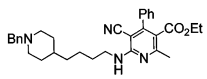 | 0.25 ± 0.02 | >10 |
| 19 | 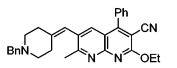 | 13.51± 1.17 | >10 |
| 20 | 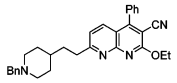 | 1.95 ± 0.38 | 8.57 ± 0.71 |
| 21 | 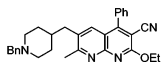 | 6.39 ± 0.75 | 6.64 ± 0.42 |

[a]Data are expressed as the mean ± SEM of at least three different experiments in quadruplicate. [b]Human recombinant AChE.[42] [c]Human serum BuChE.[42] [d]Nonsoluble.

Pyridonepezils **14**−**18** and quinolinodonepezils **20,21** were found to be selective and potent regarding the inhibition of *Ee*AChE. The length of the linker for the most potent *Ee*AChE inhibitors varies from two to four methylene units. The most potent and selective inhibitor was ethyl 6-(2-(1-benzylpiperidin-4-yl)ethylamino)-5-cyano-2-methyl-4-phenylnicotinate (**16**) [$IC_{50}$ (*Ee*AChE) = 0.0167 ± 0.0007 $\mu$M], which exhibits similar inhibitory potency as donepezil against hAChE. Compounds **17** [$IC_{50}$ (*Ee*AChE) = 0.019 ± 0.002 $\mu$M] and **18** [$IC_{50}$ (*Ee*AChE) = 0.030 ± 0.004 $\mu$M] are also potent inhibitors of *Ee*AChE. Compounds **15** [$IC_{50}$ (*Ee*AChE) = 0.79 ± 0.06 $\mu$M], and **20** [$IC_{50}$ (*Ee*AChE) = 0.10 ± 0.01 $\mu$M] are moderate AChEIs, while compound **21** shows a weak activity on *Ee*AChE [$IC_{50}$ (*Ee*AChE) = 2.7 ± 0.5 $\mu$M]. On going from compound **16** [$IC_{50}$ (eqBuChE) = 0.88 ± 0.08 $\mu$M] to **17** [$IC_{50}$


dx.doi.org/10.1021/cn300178k | ACS Chem. Neurosci. 2013, 4, 547−565

(eqBuChE) = 0.31 ± 0.05 μM], the inhibitory potency against eqBuChE is increased. Compound **18** [$IC_{50}$ (eqBuChE) = 0.380 ± 0.018 μM] shows a similar $IC_{50}$ value to **17**, which indicates that in this type of hybrid structure the presence of two or three methylene units is more suitable for BuChE inhibitory activity. The analogue **15** [$IC_{50}$ (eqBuChE) = 1.50 ± 0.08 μM] with one methylene unit is less active against eqBuChE. Quinolinodonepezils **20** and **21** are inactive against eqBuChE. We emphasize the important role accomplished by the *N*-benzylpiperidine unit on the *Ee*AChE inhibitory activity, giving support that this moiety is the main factor in mediating the binding to AChE.

*Kinetic Analysis of the AChE Inhibition by Compound **16**.* The mechanism involved in the AChE inhibition by pyridonepezils **14**–**18** was investigated using inhibitor **16**, the most potent *Ee*AChE inhibitor ($IC_{50}$ = 16.7 ± 0.2 nM) (Table 1). The type of inhibition was elucidated from the analysis of Lineweaver–Burk reciprocal plots (Figure 1) showing lines

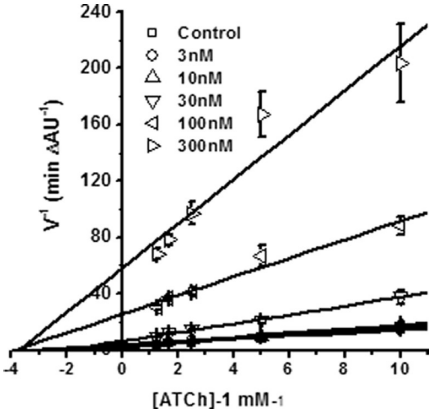


**Figure 1.** Steady-state inhibition of AChE hydrolysis of acetylthiocholine (ATCh) by compound **16**. Lineweaver–Burk reciprocal plots of initial velocity and substrate concentrations (0.1–0.8 mM) are presented. Lines were derived from a weighted least-squares analysis of data.

crossing the *x*-axis in the same point, revealing unchanged $K_m$ and decreased $V_{max}$ at increasing inhibitor concentrations. This is a typical trend for noncompetitive inhibition. A $K_i$ value of 25 nM was estimated from the slopes of double reciprocal plots versus compound **16** concentrations.

*Inhibition of Human AChE and BuChE by Compounds **14**–**21**.* Regarding the promising results achieved with *Ee*AChE and eqBuChE, pyridonepezils **14**–**18** and quinolinodonepezils **19**–**21** were also evaluated as inhibitors of human recombinant AChE (hAChE) and human serum BuChE (hBuChE) according to the protocol of Ellman et al.[51] The inhibitory activities of the hybrids were compared to those determined for the parent compound, donepezil.[42] Unfortunately, compound **14** was not soluble; thus, biological assessment was not possible. Pyridonepezils **15**–**18** were found to be selective and moderately potent regarding the inhibition of hAChE, with $IC_{50}$ values in the submicromolar range (from 0.25 to 4.57 μM, Table 2). Quinolinodonepezils **19**–**21** were found to be poor inhibitors of hAChE ($IC_{50}$ values ranged from 1.95 to 13.51 μM, Table 2). With regard to the inhibition of hBuChE, all compounds showed moderate activities in the micromolar range, being some of them inactive.

In the pyridonepezil series (**15**–**18**), the potency toward hAChE increased as the length of the linker enlarged, with ethyl 6-(4-(1-benzylpiperidin-4-yl)butylamino)-5-cyano-2-methyl-4-phenylnicotinate (**18**) being the most potent and selective toward this enzyme ($IC_{50}$ = 0.25 μM). In relation to the hBuChE inhibition, compound **16** bearing a linker of two methylenes is the most active ($IC_{50}$ = 4.00 μM), whereas other linker lengths are detrimental for the inhibition of this hydrolase. Finally, it is worth noting that compound **16** is a dual hAChE/hBuChE inhibitor. This is particularly important in view of the renewed interest in dual AChE/BuChE inhibitors as therapeutic agents for AD, since they have been described to improve cognition.[52]

*Kinetic Analysis of the AChE Inhibition by Compound **18**.* The mechanism involved in the AChE inhibition by compound **18**, the most potent hAChE inhibitor ($IC_{50}$ = 0.25 ± 0.02 μM) (Table 2), was investigated. The type of inhibition was elucidated from the analysis of Lineweaver–Burk reciprocal plots (Figure 2) showing lines crossing the *x*-axis in the same

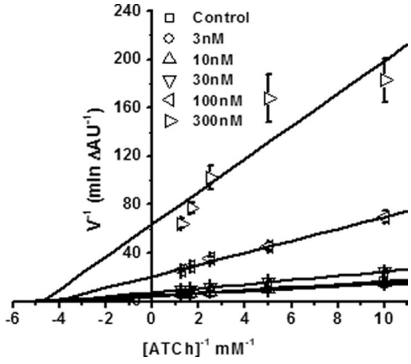


**Figure 2.** Steady-state inhibition of AChE hydrolysis of acetylthiocholine (ATCh) by compound **18**. Lineweaver–Burk reciprocal plots of initial velocity and substrate concentrations (0.1–0.8 mM) are presented. Lines were derived from a weighted least-squares analysis of data.

point, revealing unchanged $K_m$ and decreased $V_{max}$ at increasing inhibitor concentrations. This is a typical trend for noncompetitive inhibition. A $K_i$ value of 16 nM was estimated from the slopes of double reciprocal plots versus compound **18** concentrations.

The AChE from electric eel shows high homology with nerve system AChE subtypes,[53] while human erythrocyte AChE shows big differences.[54] Thus, *Ee*AChE becomes a reproducible model of CNS-located inhibition of AChE, taking into account the use of human recombinant AChE represents a very high cost, which renders its use unaffordable for kinetic experiments, as a huge amount of enzyme supply is needed for this kind of assays.

*Propidium Iodide Displacement Assay.* Compound **18** seems to inhibit AChE by a noncompetitive mechanism. To confirm whether **18** could partially interact with the PAS of AChE, experiments to evaluate the competition with propidium iodide for its binding to this site were performed. Propidium, a selective ligand for the PAS of AChE, exhibits a fluorescence increase upon binding to this site.[55] Decrease of propidium fluorescence in the presence of a compound can be interpreted as a displacement of propidium from the PAS. At 100 μM, compound **18** showed a slight but significant ability to displace propidium iodide 20 μM from the PAS of AChE (12 ± 3% over control).

*Inhibition of EeAChE and eqBuChE by Compounds 1−13.* Compounds **1−13** have been evaluated as inhibitors of *Ee*AChE and eqBuChE (Table 3) according to the protocol

**Table 3. Inhibition of *Ee*AChE/eqBuChE by Compounds 1−13**[a]

| Compound | Structure | EeAChE inhibition (% at 10 μM) | $IC_{50}$ AChE (μM) | BuChE inhibition (% at 10 μM) | $IC_{50}$ BuChE (μM) |
|---|---|---|---|---|---|
| 1 |  | 20±10 | | | 57.4±0.5 |
| 2 | 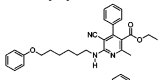 | 40±13 | | 3.7±4 | |
| 3 | 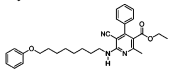 | 20±8 | | 1.4±2 | |
| 4 | 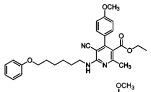 | 9±1 | | 1±1 | |
| 5 | 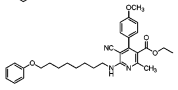 | 19±8 | | 7.4±5 | |
| 6 | 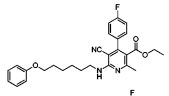 | 24±7 | | 3.5±2 | |
| 7 | 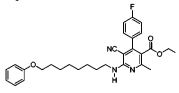 | 14±3 | | 4.4±2 | |
| 8 | 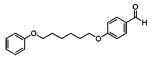 | 10±10 | | 12±2 | |
| 10 | 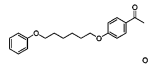 | 5±1 | | 11±3 | |
| 11 | 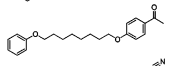 | 7±3 | | 9.4±3 | |
| 12 | 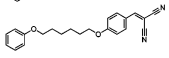 | | 6.0±0.5 | 0 | |
| 13 | 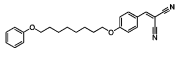 | | 2.1±0.5 | 0 | |

[a]Data are expressed as the mean ± SEM of at least three different experiments in quadruplicate.

of Ellman et al.[51] In general, these compounds were found to be poor inhibitors of both cholinesterases with the exception of compounds **12** [$IC_{50}$ (*Ee*AChE) = 6.0 ± 0.5 μM] and **13** [$IC_{50}$ (*Ee*AChE) = 2.1 ± 0.5 μM]; despite their simple structures, they showed a moderate and selective AChE inhibitory activity.

*Effect of Compounds on Neuronal Viability with MTT.* In a first step, we evaluated the potential neurotoxic effect of different compound concentrations in a neuronal cell line SH-SY5Y (human neuroblastoma cells), which allowed us to choose a concentration for each compound that is not toxic by itself. Thus, the SH-SY5Y cells were incubated with these compounds at different concentrations (5, 10, 20, 40 μM) for 24 h. Then, the cell viability was assessed by the MTT test, which determines the cells' dehydrogenase enzyme activity. Hence, cells that are metabolically impaired reduce less MTT than "healthy cells".[56,57] The phenoxyalkylamino-4-phenylnicotinates (**2−7**) and phenoxyalkoxybenzylidenemalononitriles **12,13** (Figure 3A), and pyridonepezils (**14−18**) and pyrazolo[3,4-*b*]quinolines (**35−37**) (Figure 3B) were assessed. The data obtained show that these sets of compounds did not significantly affect neuronal viability for concentrations up to 5

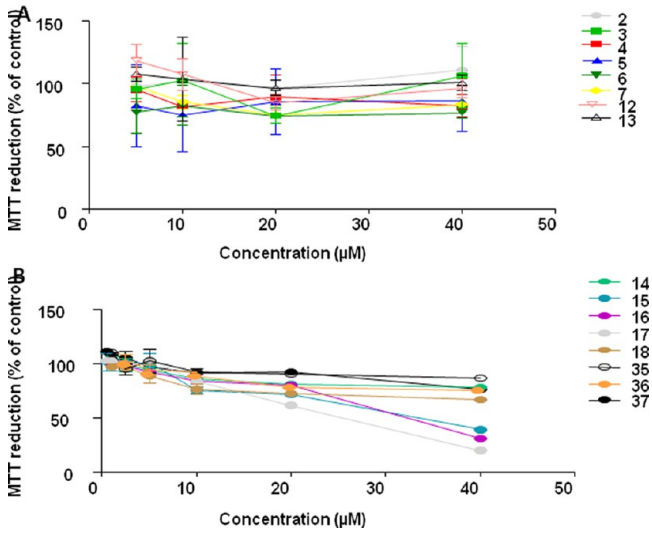


**Figure 3.** Neuronal viability, measured as reduction of MTT, in neuronal line SH-SY5Y exposed for 24 h to compounds concentrations ranging from 5 to 40 μM of the phenoxyalkylamino-4-phenylnicotinates (**2−7**) and phenoxyalkoxybenzylidenemalononitriles **12,13** (A) as well as pyridonepezils (**14−18**) and pyrazolo[3,4-*b*]quinolines (**35−37**) (B). Cell viability was evaluated by the MTT assay, as described in Methods. The data are presented as a percentage of total MTT reduced by control cells (treated with 0.1% DMSO, the compound vehicle). Data are mean ± SEM of three independent experiments done in duplicate.

μM, whereas for higher concentrations the compounds affected the neuronal viability by 15% or more. Thus, in the following experiments, the compounds were used at concentrations that per se were not toxic.

*Neuroprotection against Aβ-Toxicity.* The potential neuroprotective effect of phenoxyalkylamino-4-phenylnicotinates (**2−7**), phenoxyalkoxybenzylidenemalononitriles (**12,13**), pyridonepezils (**14−18**), and pyrazolo[3,4-*b*]quinolines (**35−37**) against neuronal injury triggered by $A\beta_{1-42}$ (2 μM incubated for 24h) was evaluated (Figure 4). The peptide $A\beta_{1-42}$ (2 μM) incubated for 24 h caused per se a decrease of about 30% in neuronal viability; that is, the cells exposed to $A\beta_{1-42}$ reduced only 68.7 ± 1.7% of the MTT in contrast to the about 100% MTT reduction observed in control cells (cells treated with 0.1% DMSO, used as a vehicle). The decrease in cell viability caused by $A\beta_{1-42}$ was significantly ($p < 0.05$) prevented by compounds **2**, **7**, and **13** (10 μM), whereas compounds **3** and **6** displayed a slightly neuroprotective effect against Aβ. In contrast, compounds **4**, **5**, and **12** did not protect against $A\beta_{1-42}$ neurotoxicity (Figure 4A). We have also tested the potential neuroprotective role of compounds **14−18** (2.5 μM) and **35−37** (5 μM) against $A\beta_{1-42}$, incubated for 24 h (Figure 4B). As can be seen in Figure 4B only compounds **17**, **18**, **35**, and **36** were able to prevent Aβ-neurotoxicity ($p < 0.05$). Compounds **14−16** and **37** caused a slight protection without statistical significance ($p > 0.05$).

*Impact on the Enhancement of AChE Activity Caused by Aβ Peptides.* Since some of these compounds can have anticholinesterase activity, we evaluated whether the phenoxyalkylamino-4-phenylnicotinates (**2−7**), phenoxyalkoxybenzylidenemalononitriles (**12,13**), pyridonepezils (**14−18**), and pyrazolo[3,4-*b*]quinolines (**35−37**) were able to prevent the increase in AChE activity (Figure 5) caused by $A\beta_{1-42}$ (2 μM incubated for 24 h) in the neuronal cell line SH-SY5Y, which


dx.doi.org/10.1021/cn300178k | *ACS Chem. Neurosci.* 2013, 4, 547−565

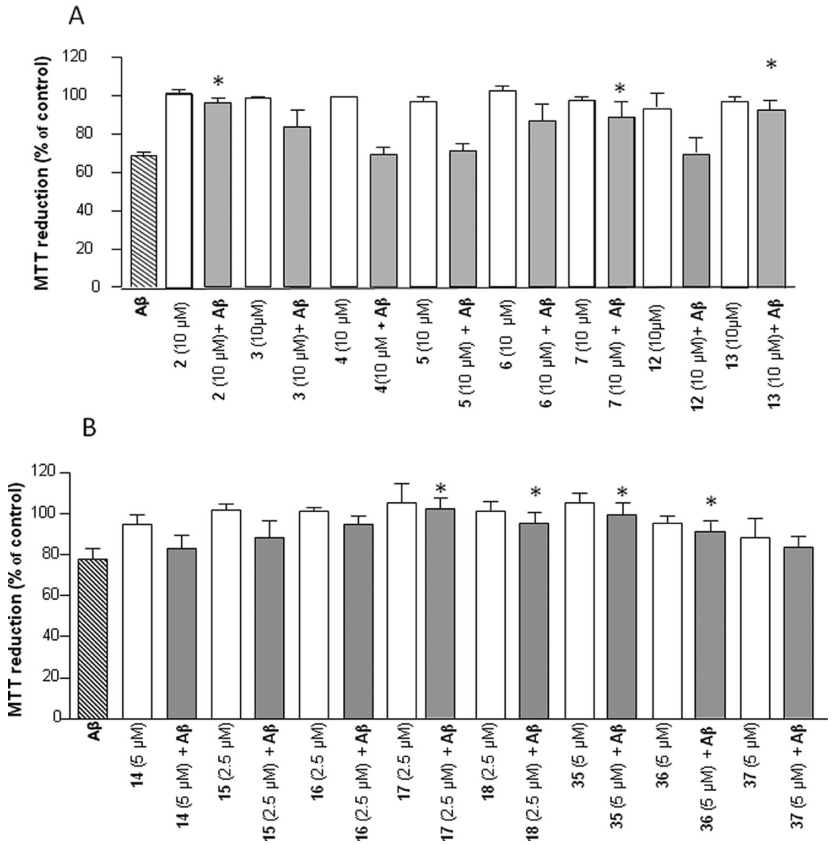


**Figure 4.** Assessment of the neuroprotective effect of phenoxyalkylamino-4-phenylnicotinates (**2**−**7**) and phenoxyalkoxybenzylidenemalononitriles (**12**,**13**) (A), as well as of pyridonepezils (**14**−**18**) and pyrazolo[3,4-*b*]quinolines (**35**−**37**) (B) in the neuronal injury triggered by A$\beta_{1-42}$. The neuronal cell line SH-SY5Y was exposed to the cited compounds concentrations in the presence or absence of A$\beta_{1-42}$ (2 $\mu$M) for 24 h (see Methods). Then, cell viability was evaluated by the MTT assay, as described in Methods, and the data are presented as a percentage of total MTT reduced by control cells (treated with 0.1% DMSO, the compound vehicle). Data are mean ± SEM of three to six independent experiments done in duplicate.

were shown to have AChE.[58] We have previously reported that A$\beta$ peptides are able to increase AChE in cultured neuronal cells.[57] In this study, we also observed that A$\beta_{1-42}$ peptide enhanced AChE activity by about 20%. The phenoxyalkylamino-4-phenylnicotinates (**2**−**5** and **7**) caused a significant ($p$ < 0.05) reduction in the AChE activity, whereas compound **6** did not affect significantly this enzyme (Figure 5A). All compounds were effective in preventing the enhancement of AChE activity induced by A$\beta_{1-42}$, which is the AChE activity in neurons challenged to A$\beta_{1-42}$. The pyridonepezils **17** and **18** decreased the activity by 50% and 30%, respectively, whereas compound **16** caused a significant reduction of about 12% in AChE activity of cells challenged to A$\beta_{1-42.}$ Regarding the pyrazolo[3,4-*b*]quinolines (**35**−**37**), we observed that compounds **36** and **38**, but not compound **35**, caused a significant ($p$ < 0.05) inhibition in AChE, preventing the upregulation of this enzyme induced by A$\beta_{1-42}$ (Figure 5B).

*Effect of Compounds in Intracellular $Ca^{2+}$ Homeostasis Dysregulation.* Disruptions in $Ca^{2+}$ homeostasis are implicated in diverse disease processes and have become a major focus of study in multifactorial neurodegenerative disorders such as AD. Since no cure is currently known, targeting $Ca^{2+}$ dyshomeostasis as an underlying and integral component of AD pathology may result in novel and effective treatments for AD.[32] The phenoxyalkylamino-4-phenylnicotinates (**2**,**3**,**7**), the phenoxyalkoxybenzylidenemalononitriles (**12**,**13**), the pyridonepezils (**16**−**18**), and the pyrazolo[3,4-*b*]quinolines (**35**−**37**) were evaluated as potential antagonists of voltage sensitive calcium channels (VSCC). Thus, we tested the cited compounds in the $Ca^{2+}$ influx evoked by 50 mM KCl in neuronal cells (Figure 6), which cause depolarization and the opening of VSCC. It should be referred that cells challenged to A$\beta_{1-42}$ had increased basal intracellular $Ca^{2+}$ levels, so when these cells were $K^+$-depolarized the influx of $Ca^{2+}$ was lower than in control cells and the effects of compounds were not detectable (data not shown) . However, when compounds **2**, **7**, **12**, **13**, **17**, **18**, and **36** were tested in control cells, it was observed that they significantly prevented the $Ca^{2+}$ influx evoked by KCl (50 mM) depolarization, suggesting that these set of compounds can act as antagonists of VSCC.

Previous studies also demonstrated donepezil might have a neuroprotective effect by inhibition of $Ca^{2+}$ channels, as it was reported to inhibit the high potassium-induced $[Ca^{2+}]_i$ rise at high concentrations[59] and block voltage-gated calcium channels in molluscan neurons with the $IC_{50}$ value of 7.9 $\mu$M.[60]

*Molecular Modeling Studies.* In silico molecular modeling studies were undertaken to gain insight into the interaction of compound **16** with the residues of the ligand binding sites of the *Ee*AChE and eqBuChE proteins and into the interaction of compounds **16** and **18** with the residues of the ligand binding sites of the hAChE and hBuChE proteins. The 3D structures of the corresponding enzymes were employed since ligands bind to enzyme species differently despite the high homology sequence among species. The technique of blind docking was


dx.doi.org/10.1021/cn300178k | *ACS Chem. Neurosci.* 2013, 4, 547−565

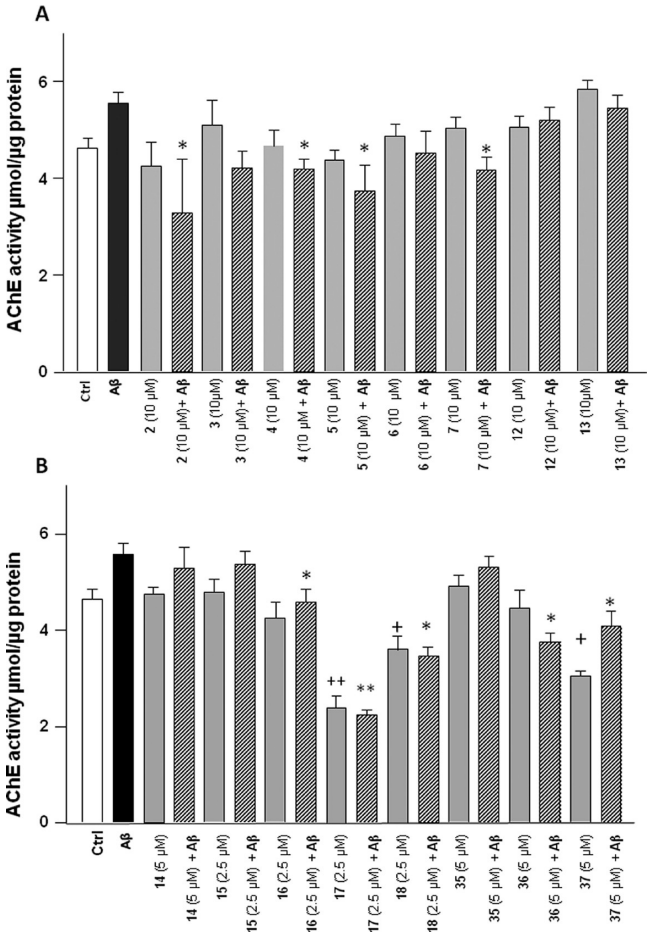


**Figure 5.** Assessment of the phenoxyalkylamino-4-phenylnicotinates (**2**–**7**) and phenoxyalkoxybenzylidenemalononitriles (**12**,**13**) (A), as well as pyridonepezils (**14**–**18**) and pyrazolo[3,4-*b*]quinolines (**35**–**37**) (B), in AChE activity in neuronal cells exposed or not to A$\beta_{1-42}$. The neuronal cell line SH-SY5Y was exposed to the cited compounds concentrations in the presence or absence of A$\beta_{1-42}$ (2 $\mu$M) for 24 h (see Methods). Then, the AChE activity was evaluated as described in Methods, and the data are presented as $\mu$mol of acetylthiocholine iodide hydrolyzed/$\mu$g of protein. Data are mean ± SEM of three to six independent experiments done in duplicate.

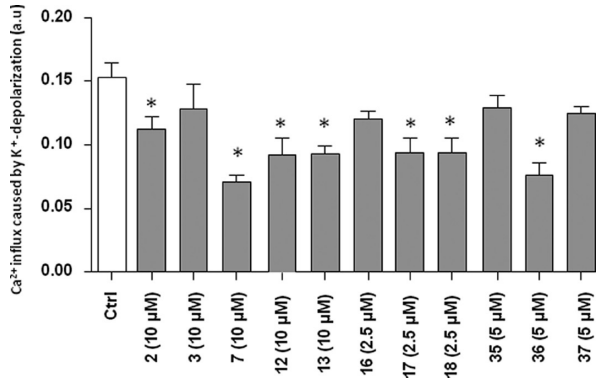


**Figure 6.** Influx of $Ca^{2+}$ triggered by KCl (50 mM) depolarization in neuronal cells (SH-SY5Y) in the presence of compounds **2**, **3**, **7**, **12**, **13**, **16**–**18**, and **35**–**37**. Control cells were treated with 0.1% DMSO, the compound vehicle. The intracellular $Ca^{2+}$ levels were measured, using the fura-2 fluorescent dye, and the fluorescence was measured at $\lambda$ of 340, 380 excitation and 510 nm emission (see Methods). The $Ca^{2+}$ influx was calculated as the difference between peak of fura-2 fluorescence upon depolarization and the basal fura-2 fluorescence. Data are mean ± SEM of three to four independent experiments and expressed as arbitrary units (a.u.) of fluorescence.

used for the detection of possible binding sites and modes of peptide ligands by scanning the entire surface of protein targets so that a location with the highest binding affinity on the proteins may be found.

The program AutoDock Vina[61] was used to perform the blind docking using a single catalytic subunit of *Ee*AChE (PDB: 1C2B) and hAChE complexed with fasciculin-II (PDB: 1B41). To account for flexibility during docking, flexible torsion in the ligand was assigned, and the dihedral angles were allowed to rotate freely. The demand to account for protein flexibility in docking schemes is widely accepted because it has been found that small movements in the side chain or backbone of the protein can be enough either to increase or decrease the size of the active site, or to alter the hydrogen-bonding pattern between protein and ligand. The incorporation of protein structural flexibility into the ligand generation procedure has been commonly used in our AChE studies.[43,62−64] In particular, when the ligands are large and bulky, Trp286, Tyr124, Tyr337 and Tyr72, Asp74, Thr75, Trp86, and Tyr341 receptor residues have been selected to be flexible during docking simulation.[65]

These eight residues delineate the shape of the gorge entry and lining, as their motion may significantly enlarge the gorge mouth to facilitate ligand access to the catalytic site.

Compound **16** was modeled into the structure of *Ee*AChE, and the visual inspection of the top scored pose reveals that the ligand is accommodated at the active-site gorge (Figure 7A). It has been observed that $\pi-\pi$ interactions played an important role in stabilizing the complex. The ligand interacts with Tyr341 and Trp286 (PAS) forming a face-to-face $\pi-\pi$ interaction with the pyridine moiety. The hydrophobic interaction between **16** (the piperidine and the alkyl linker) and the rich aromatic residues (Tyr124, Tyr337, Phe338, Tyr341, and Phe297) along the gorge could direct the phenyl ring to penetrate into the anionic site and oxyanion hole regions in the choline-binding site (Figure 7B). These interactions could possibly help to dock the phenyl moiety of the ligand to the anionic subsite by $\pi-\pi$ stacking interaction between Trp86 (AS) and the phenyl moiety. Additionally, **16** is able to form a hydrogen bond between the secondary amine function of the linker and the hydroxyl group of Tyr124 residue.

Compound **16** was also modeled into the structure of BuChE. In the absence of the X-ray structure of eqBuChE, a homology model was used to rationalize the experimental data. The modeling of the 3D structure was performed by using an automated homology-modeling program[67−69] (SWISS-MODEL). A putative three-dimensional structure of eqBuChE has been created based on the crystal structure of hBuChE (pdb: 2PM8) as these two enzymes exhibited 89% sequence identity.

Docking experiments were performed as blind dockings following the same computational protocol used for *Ee*AChE. The best-ranked docking solutions revealed that eqBuChE could effectively accommodate compound **16** inside the active site gorge (Figure 8A). The **16**-eqBuChE complex was stabilized mainly by hydrophobic interactions including those established with the amino acid residues of both CAS and PAS of the enzyme (Figure 8B). Another interaction to consider


dx.doi.org/10.1021/cn300178k | *ACS Chem. Neurosci.* 2013, 4, 547−565

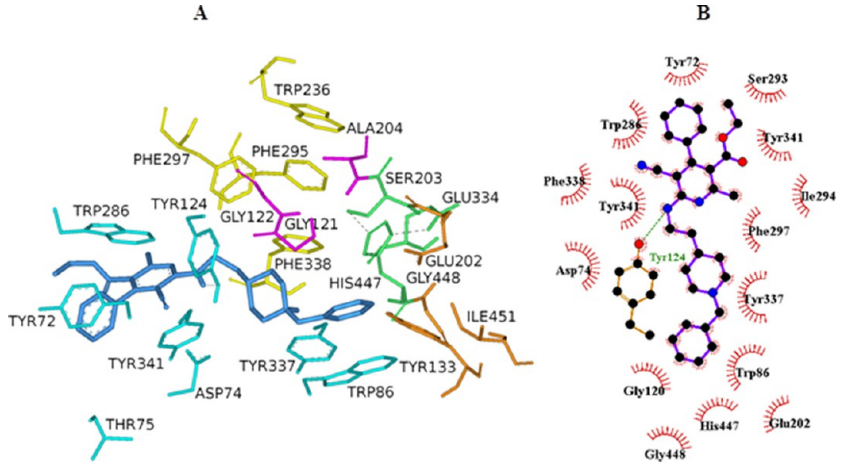


**Figure 7.** Binding mode of 16 at the active site of *Ee*AChE. (A) The compound is rendered as sticks and illustrated in blue. The side chains conformations of the mobile residues are illustrated in the same color (light blue) of the ligand. Different subsites of the active site are colored: catalytic triad (CT) in green, oxyanion hole (OH) in pink, anionic subsite (AS) in orange except Trp86, acyl binding pocket (ABP) in yellow, and peripheral anionic subsite (PAS) in blue. (B) Schematic diagram of protein–ligand interactions generated by LIGPLOT.[66] Brown stick models present the residues of the enzymes, purple stick models present the inhibitor, hydrogen bonds are green dashed lines, and hydrophobic contacts with the ligand are presented by red semicircles with radiating spokes.

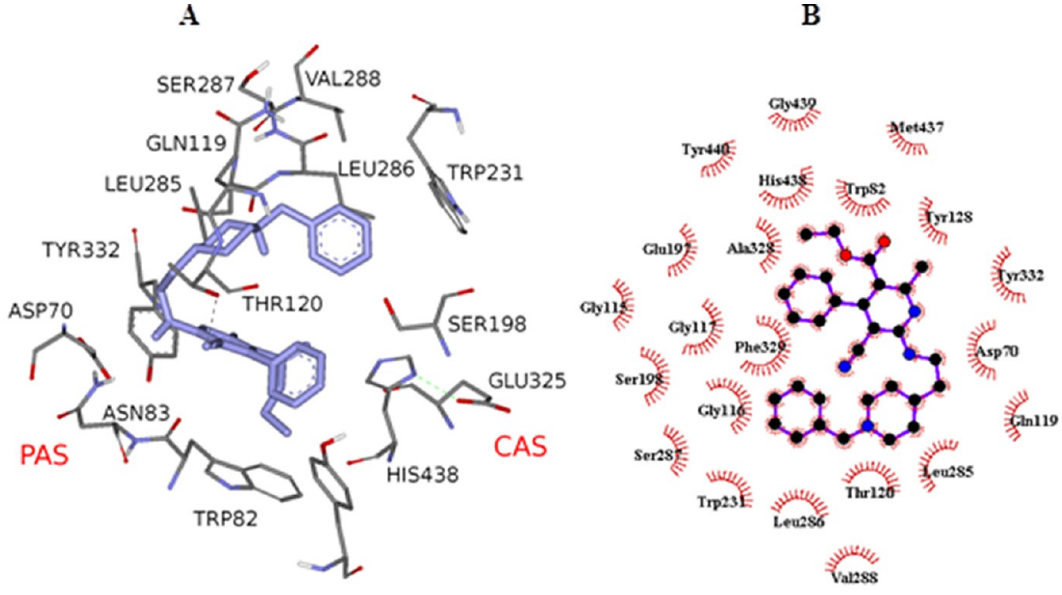


**Figure 8.** Close view of the potential interaction between **16** and the binding site of eqBuChE homology built 3D-model. (A) Complex of compound **16** (violet) and eqBuChE. Hydrogen bonds are represented as black dashed lines. (B) Intermolecular hydrophobic interactions of **16** with eqBuChE in 2D flattened space generated by LIGPLOT. Purple stick models present the inhibitor, and hydrophobic contacts with the ligand are presented by red semicircles with radiating spokes.

would be the hydrogen bond established between THR120 and the cyano group of the ligand (Figure 8A).

The orientation and conformation of **16** in *Ee*AChE were completely different from those in eqBuChE. The ligand binds to *Ee*AChE with an extended conformation whereas it binds to eqBuChE with a folded conformation (Figure 9). The docking calculation of **16** at the active sites of *Ee*AChE and eqBuChE revealed that the compound bounds to the *Ee*AChE enzyme with lower binding energy (−11.6 kcal/mol) when compared with eqBuChE enzyme (−9.2 kcal/mol). Besides, the energy of the bioactive conformation in eqBuChE is higher than that in *Ee*AChE. Therefore, the energetic and structural features of the corresponding **16**-enzyme complexes can be, at least in part, the

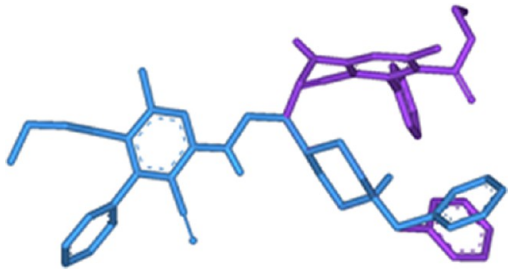

**Figure 9.** Superposition of the bioactive conformations for compound **16** in *Ee*AChE (blue sticks) and in eqBuChE (violet sticks).


dx.doi.org/10.1021/cn300178k | *ACS Chem. Neurosci.* 2013, 4, 547–565

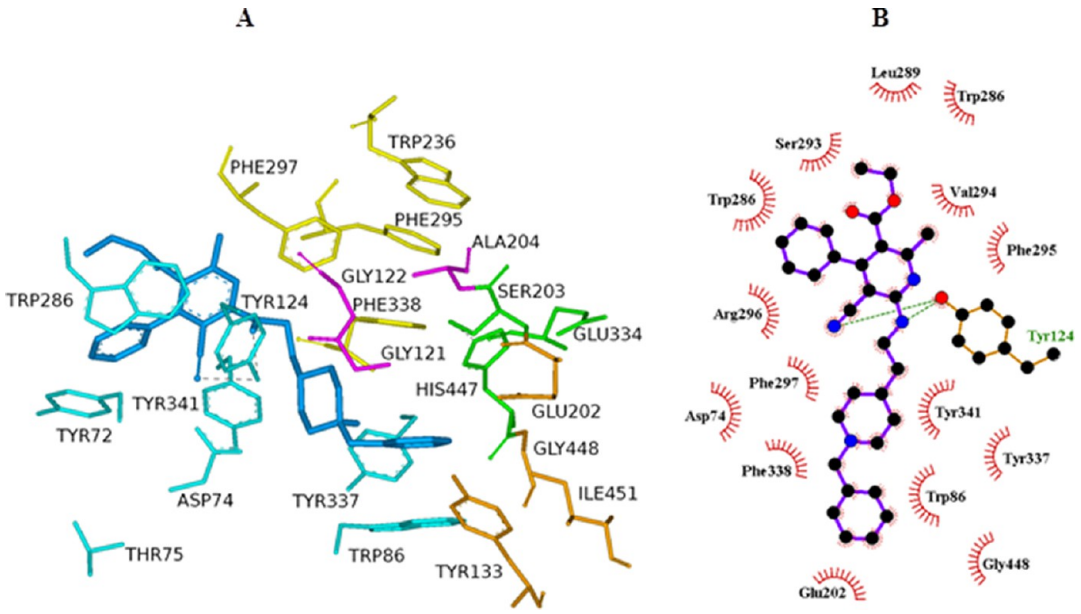


**Figure 10.** Binding mode of **16** at the active site of hAChE. (A) The compound is rendered as sticks and illustrated in blue. The side chains conformations of the mobile residues are illustrated in the same color (light blue) of the ligand. Different subsites of the active site are colored: catalytic triad (CT) in green, oxyanion hole (OH) in pink, anionic subsite (AS) in orange except Trp86, acyl binding pocket (ABP) in yellow, and peripheral anionic subsite (PAS) in blue. (B) Intermolecular hydrophobic interactions of **16** with hAChE in 2D flattened space generated by LIGPLOT.[66] Purple stick models present the inhibitor, and hydrophobic contacts with the ligand are presented by red semicircles with radiating spokes. Hydrogen bonds are green dashed lines.

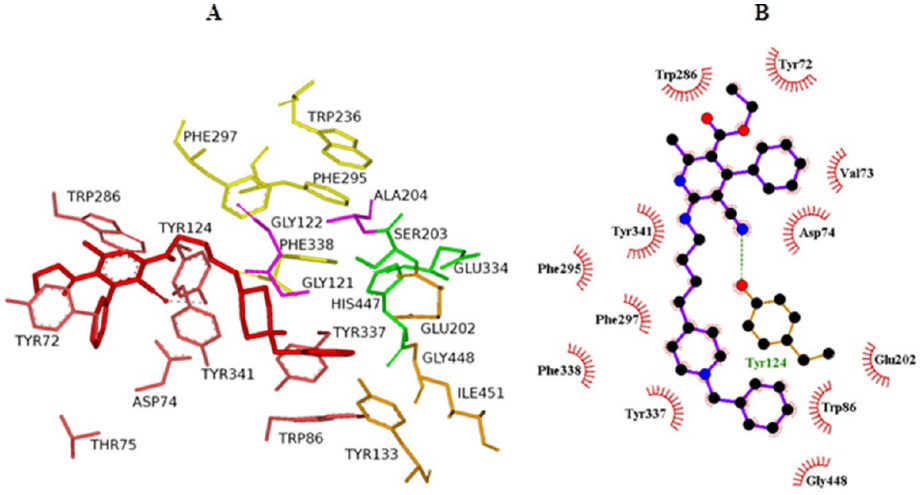


**Figure 11.** Binding mode of 18 at the active site of hAChE. (A) The compound is rendered as sticks and illustrated in red. The side chains conformations of the mobile residues are illustrated in the same color (light red) of the ligand. Different subsites of the active site are colored: catalytic triad (CT) in green, oxyanion hole (OH) in pink, anionic subsite (AS) in orange except Trp86, acyl binding pocket (ABP) in yellow,and peripheral anionic subsite (PAS) in red. (B) Schematic diagram of protein−ligand interactions generated by LIGPLOT.[66] Brown sticks models present the residues of the enzymes, purple stick models present the inhibitor, hydrogen bonds are green dashed lines, and hydrophobic contacts with the ligand are presented by red semicircles with radiating spokes.

reason why compound **16** shows lower eqBuChE inhibitory activity than *Ee*AChE inhibitory activity.

Blind docking simulations were also carried out with the software Autodock Vina[61] using hAChE complexed with fasciculin-II (PDB: 1B41). Docking experiments were performed following the same computational protocol used for *Ee*AChE.

The top scored pose of **16** reveals that the ligand is accommodated at the active-site gorge (Figure 10A). Compound **16** is positioned into the hAChE binding site almost at the same place occupied by **16** into the *Ee*AChE binding site. In particular, the following major interactions, responsible for the inhibiting profile of the selected molecule, could be identified: (i) The ligand interacts with Tyr341 and Trp286 (PAS) forming a face-to-face $\pi-\pi$ interaction with the cyano-pyridine moiety; (ii) the hydrophobic interaction between **16** (the piperidine and the alkyl linker) and the rich aromatic residues (Tyr124, Tyr337, Tyr341, Phe338, and Phe297) along the gorge (Figure 10B); (iii) the cyano group can establish H-bond interaction with the hydroxyl group of Tyr133; (iv) the secondary amino group of the linker donates a proton to the hydroxyl group of Tyr124 and forms a hydrogen


dx.doi.org/10.1021/cn300178k | *ACS Chem. Neurosci.* 2013, 4, 547−565

bond; (v) the phenyl ring interacts with Trp86 (AS) by means of a $\pi-\pi$ stacking

Docking of compound **18** in the hAChE structure showed that the compound was positioned in a similar orientation to that of compound **16** (Figure 11A). The benzylpiperidine moiety adopted a similar rearrangement in both cases, and little structural fluctuations were also found in midgorge and pheripheral sites for complexes **16**-hAChE and **18**-hAChE, in the alkyl linker and in the pyridine moiety. The cyano-pyridine moiety still interacts with the PAS through a $\pi-\pi$ interaction with Trp 286 and Tyr341, and the cyano group is hydrogen-bonded with the hydroxyl hydrogen of Tyr124. This hydrogen bond and the hydrophobic interaction between **18** (the piperidine and the alkyl linker) and the rich aromatic residues (Tyr124, Tyr337, Tyr341, Phe338, Phe297, and Phe295) along the gorge could aid to the phenyl ring to engage in a $\pi-\pi$ stacking interaction with the indole ring of Trp 86 (Figure 11B). At the lip of the gorge, the phenyl moiety gives a face-to-edge polarized $\pi-\pi$ interaction with Tyr72. For compound **18**, hydrogen bond interaction of the amine function of the linker with Tyr124 was not found.

According to the above descriptions, the ligand **18** binds to hAChE and the ligand **16** to both the EeAChE and the hAChE, in an extended conformation from the mouth to the central region of the active site gorge, but no interactions with the catalytic triad residues have been found. These results suggest that compounds **16** and **18** could favorably interact with the PAS but not with the catalytic site of AChE; therefore, docking results are in agreement with the experimental kinetic data, indicating a noncompetitive inhibition.

Docking experiments for compounds **16** and **18** into the structure of hBuChE (PDB: 1P0I) were performed as blind dockings following the same computational protocol used for eqBuChE. The best-ranked docking solutions revealed that hBuChE could effectively accommodate compounds **16** and **18** inside the active site gorge (Figure 12). The **16**-hBuChE and

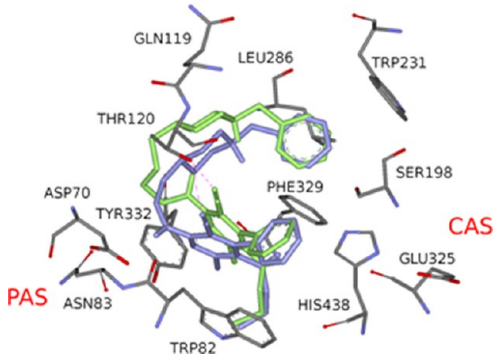


**Figure 12.** Close view of the potential interaction between **16** and **18** and the binding site of hBuChE. The compounds are rendered as sticks, compound **16** is illustrated in violet, and compound **18** in green. Hydrogen bonds are represented as pink dashed lines.

**18**-hBuChe complexes were stabilized mainly by hydrophobic interactions including those established with the amino acid residues of both CAS and PAS of the enzyme (Figure 13).

Another interaction to consider would be the hydrogen bond established between Thr120 and the cyano group of the ligands (Figures 12 and 13).

The orientations and conformations of **16** and **18** in AChE were completely different from those in BuChE. The ligands bind to AChE with extended conformations, whereas they bind to BuChE with folded conformations (Figure 14). The docking calculation of **16** and **18** at the active sites of AChE and BuChE revealed that the compounds bound to the AChE enzyme with lower binding energy when compared with BuChE enzyme. For compound **16**, the energy gap in hBuChE is approximately 38 kcal/mol higher than that calculated for the hAChE. In the case of compound **18**, the value is increased to 181 kcal/mol. This energetic penalty can be, at least in part, the reason why both ligands show low hBuChE inhibitory activity, with compound **18** being more selective.

## CONCLUSIONS

The synthesis and biological activity of phenoxyalkylamino-4-phenylnicotinates (**2**–**7**), phenoxyalkoxybenzylidenemalononitriles (**12**,**13**), pyridonepezils (**14**–**18**), and quinolinodonepezils (**19**–**21**) were reported. Additional biological activity on pyrazolo[3,4-*b*]quinolines (**35**–**37**)[50] is reported. Pyridonepezils **15**–**18** were found to be selective and moderately potent regarding the inhibition of hAChE. $IC_{50}$ values were similar in a few cases (ranging from 0.25 to 4.57 $\mu$M), whereas quinolinodonepezils **19**–**21** were found to be poor inhibitors of hAChE. ($IC_{50}$ values ranged from 1.95 to 13.51 $\mu$M.) The most potent and selective hAChE inhibitor was ethyl 6-(4-(1-benzylpiperidin-4-yl)butylamino)-5-cyano-2-methyl-4-phenylnicotinate (**18**) [$IC_{50}$ (hAChE) = 0.25 ± 0.02 $\mu$M]. Pyridonepezils **15**–**18** and quinolinodonepezils **20**,**21** are more potent selective inhibitors of *Ee*AChE than hAChE ($IC_{50}$ values ranging from 0.0167 to 2.7 $\mu$M). The length of the linker for the most potent hAChE and *Ee*AChE inhibitors varies from two to four methylene units, but, in the case of *Ee*AChE, the most potent and selective inhibitor was ethyl 6-(2-(1-benzylpiperidin-4-yl)ethylamino)-5-cyano-2-methyl-4-phenylnicotinate (**16**) [$IC_{50}$ (*Ee*AChE) = 0.0167 ± 0.0007 $\mu$M], which exhibits the same inhibitory potency as donepezil against hAChE. In general, pyridonepezils **15**–**18** and quinolinodonepezils **20**,**21** are also more potent to eqBuChE than to hBuChE, as $IC_{50}$ values range from 0.31 to 10 $\mu$M. Cell viability measured as MTT reduction showed that exposure of SH-SY5Y cells during 24 h with 5 $\mu$M of the phenoxyalkylamino-4-phenylnicotinates (**2**–**7**), the phenoxyalkoxybenzylidenemalononitriles (**12**,**13**), the pyridonepezils (**14**–**18**), and the pyrazolo[3,4-*b*]quinolines (**35**–**37**) did not significantly affect neuronal viability. Moreover, the decrease in cell viability caused by A$\beta_{1-42}$ was significantly prevented by compounds **2**, **7**, and **13** (10 $\mu$M), **17** (2.5 $\mu$M), **18** (2.5 $\mu$M), **35** (5 $\mu$M), and **36** (5 $\mu$M). In this study A$\beta_{1-42}$ peptide was also examined to enhance AChE activity by about 20%. All compounds were effective in preventing the enhancement of AChE activity induced by A$\beta_{1-42}$. The phenoxyalkylamino-4-phenylnicotinates (**2**–**5** and **7**) caused a significant reduction, whereas compound **6** did not affect substantially this enzyme. The pyridonepezils **17** and **18** decreased the activity by 50% and 30%, respectively, whereas compound **16** caused a reduction of about 12%. The pyrazolo[3,4-*b*]quinolines **36** and **38** also prevented the upregulation of AChE induced by A$\beta_{1-42}$. At 100 $\mu$M, compound **18**, which seems to inhibit AChE by a noncompetitive mechanism, showed a slight but significant ability to displace propidium iodide 20 $\mu$M from the PAS of AChE (12 ± 3% over control) in the propidium iodide displacement assay. It was observed that compounds **2**, **7**, **12**, **13**, **17**, **18**, and **36** expressively prevented the $Ca^{2+}$ influx evoked by KCl (50 mM) depolarization, suggesting that this set

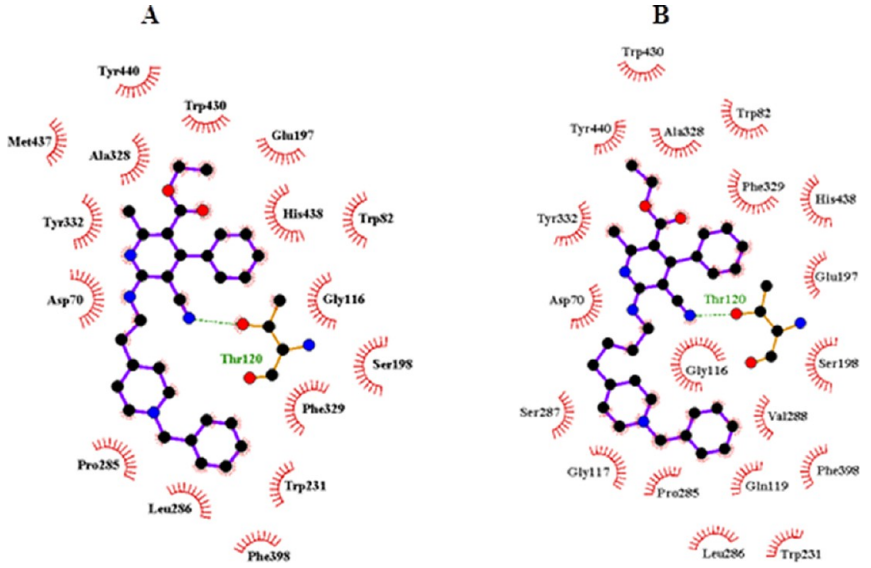


**Figure 13.** Schematic diagram of protein−ligand interactions generated by LIGPLOT.[66] (A) Interactions of compound **16** with BuChE. (B) Interactions of compound **18** with BuChE. Brown sticks models present the residues of the enzymes, purple stick models present the inhibitor, hydrogen bonds are green dashed lines, and hydrophobic contacts with the ligand are presented by red semicircles with radiating spokes.

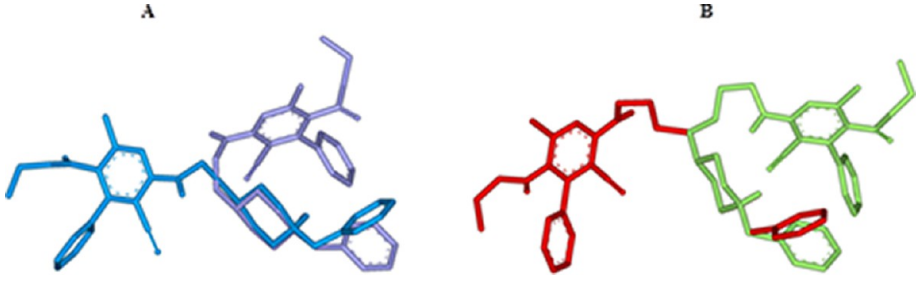


**Figure 14.** (A) Superposition of the bioactive conformations for compound **16** in hAChE (blue sticks) and in hBuChE (violet sticks). (B) Superposition of the bioactive conformations for compound **18** in hAChE (blue sticks) and in hBuChE (green sticks).

of compounds can act as antagonists of VSCC. Compounds **16** and **18** were found to adopt different orientations and conformations inside the active-site gorges of hAChE and hBuChE. Compound **16** showed a binding geometry in *Ee*AChE very similar to the one displayed by the compound in hAChE. The structural and energetic features of the ligand-AChE complex compared to the ligand-BuChE complex account for a higher affinity of the ligands toward AChE. For ligands **16** and **18**, the energy of the bioactive conformation in BuChE is higher than that in AChE. This energy difference is much higher for compound **18** which may explain its selectivity. To conclude, the present data indicate that compounds **2**, **7**, **17**, **18**, and **36** are attractive multipotent molecules acting in different key pharmacological targets. Thus, they may accomplish a potential disease-modifying role in the treatment of AD.

## METHODS

**Chemistry.** *General Methods.* Melting points were determined on a Koffler apparatus, and are uncorrected. $^{1}$H NMR and $^{13}$C NMR spectra were recorded in $CDCl_3$ or DMSO-$d_6$ at 300, 400, or 500 MHz and at 75, 100, or 125 MHz, respectively, using solvent peaks [$CDCl_3$: 7.27 (*D*), 77.2 (*C*) ppm; $D_2O$: 4.60 ppm and DMSO-$d_6$: 2.49 (*D*), 40 (*C*) ppm] as internal reference. The assignment of chemical shifts was based on standard NMR experiments ($^{1}$H, $^{13}$C-DEPT, $^{1}$H, $^{1}$H−COSY, gHSQC, gHMBC). Mass spectra were recorded on a GC/MS spectrometer with an API-ES ionization source. Elemental analyses were performed at CNQO (CSIC, Spain). TLC was performed on silica F254, and detection by UV light was conducted at 254 nm or by charring with either ninhydrin, anisaldehyde, or phosphomolybdic-$H_2SO_4$ dyeing reagents. Anhydrous solvents were used in all experiments. Column chromatography was performed on silica gel 60 (230 mesh). "Chromatotron" separations were performed on a Harrison Research model 7924 Chromatotron equipped with a UV Lamp. The circular disks were coated with Kieselgel 60 PF254 (E. Merck).

*General Procedure for the Synthesis of 6-((n-Benzylpiperidin-4-yl)alkylamino)-5-cyano-2-methyl-4-phenylnicotinates.* To a solution of ethyl 6-chloro-5-cyano-2-methyl-4-phenylnicotinate[41] and triethylamine in THF/EtOH 3:1 (v/v) or acetonitrile, the respective amino-benzylpiperidine was added and the mixture was refluxed. When the reaction was complete, the solvent was removed and the crude was purified by flash chromatography.

*Ethyl 6-(1-Benzylpiperidin-4-ylamino)-5-cyano-2-methyl-4-phenylnicotinate (**14**).* Following the general procedure, ethyl 6-chloro-5-cyano-2-methyl-4-phenylnicotinate (**22**)[41] (100 mg, 0.33 mmol), triethylamine (0.9 mL, 6.46 mmol), commercial 4-amino-1-benzylpiperidine (**23**) (0.08 mL, 0.38 mmol), in THF/EtOH 3:1 (v/v) (4 mL), after 25 h, followed by flash chromatography (*n*-hexane/ethyl acetate 40%), afforded compound **14** (100 mg, 66%): mp 213−5 °C; IR (KBr) $\nu_{max}$ 3341, 2946, 2806, 2764, 2222, 1710, 1572, 1558, 1513, 1492, 1470, 1456, 1362 cm$^{-1}$; $^{1}$H NMR (400 MHz, $CDCl_3$) $\delta$ 7.61−7.27 (m, 10H, phenyl groups), 5.26 (d, $J$ = 7.6 Hz, 1H, NH), 4.31−4.05 (m, 1H, H-4′″ piperidyl), 3.92 (q, $J$ = 7.1 Hz, 2H, $OCH_2CH_3$), 3.55 (s, 2H, $CH_2Ph$), 2.87 (d, $J$ = 11.8 Hz, 2H, H-2′″, H-6′″ piperidyl), 2.52 (s, 3H, $CH_3$ pyridyl), 2.23 (t, $J$ = 10.5 Hz, 2H, H-2′″, H-6′″


dx.doi.org/10.1021/cn300178k | *ACS Chem. Neurosci.* 2013, 4, 547−565

piperidyl), 2.06 (dd, $J$ = 12.3, 3.8 Hz, 2H, H-3′″, H-5′″ piperidyl), 1.79−1.49 (m, 2H H-3′″, H-5′″ piperidyl), 0.83 (t, $J$ = 7.1 Hz, 3H, $OCH_2CH_3$); $^{13}C$ NMR (101 MHz, $CDCl_3$) $\delta$ 167.9 (C═O), 161.0 (C-2 py), 157.5 (C-6 py), 154.1 (C-4 py), 138.4 (C-1″ $CH_2Ph$), 136.6 (C-1′ Ph), 129.4 (C-3′, C-4′, C-5′ Ph), 128.7 (C-2″, C-6″ $CH_2Ph$), 128.5 (C-3″, C-5″ $CH_2Ph$), 128.0 (C-2′, C-6′ Ph), 127.3 (C-4″ $CH_2Ph$), 118.4 (C-3 py), 116.5 (CN), 89.2 (C-5 py), 63.3 ($CH_2Ph$), 61.3 ($OCH_2CH_3$), 52.3 (C-2′″, C-6′″ piperidyl), 48.4 (C-4′″ piperidyl), 32.3 (C-3′″, C-5′″ piperidyl), 24.3 ($CH_3$ pyridyl), 13.7 ($OCH_2CH_3$); MS (ESI) $m/z$: 477 $(M+Na)^+$, 455 $(M+H)^+$. Anal. Calcd. for $C_{28}H_{30}N_4O_2$: C, 73.98; H, 6.65; N, 12.33. Found: C, 73.85; H, 6.91; N, 12.16.

*Ethyl 6-((1-Benzylpiperidin-4-yl)methylamino)-5-cyano-2-methyl-4-phenylnicotinate (**15**).* Following the general procedure, ethyl 6-chloro-5-cyano-2-methyl-4-phenylnicotinate (**22**)[41] (84 mg, 0.28 mmol), triethylamine (0.47 mL, 3.37 mmol), (1-benzylpiperidin-4-yl)methanamine (**24**)[42] (67 mg, 0.33 mmol), in THF/EtOH 3:1 (v/v) (4 mL), after 65 h, followed by flash chromatography (*n*-hexane/ethyl acetate 50%), afforded compound **15** (97.3 mg, 74%): mp 170−2 °C; IR (KBr) $\nu_{max}$ 3375, 2921, 2806, 2749, 2217, 1721, 1580, 1560, 1493, 1456, 1444 $cm^{-1}$; $^1H$ NMR (300 MHz, $CDCl_3$) $\delta$ 7.58−7.29 (m, 10H), 5.45 (t, $J$ = 5.6 Hz, 1H, NH), 3.92 (q, $J$ = 7.1 Hz, 2H, $OCH_2CH_3$), 3.59−3.43 (m, 4H, $CH_2Ph$ + $CH_2NH$), 2.93 (d, $J$ = 11.4 Hz, 2H, H-2, H-6 piperidyl), 2.52 (s, 3H, $CH_3$ py), 2.00 (dd, $J$ = 20.4, 9.0 Hz, 2H, H-3′″, H-5′″ piperidyl), 1.74 (d, $J$ = 13.3 Hz, 2H, H-3′″, H-5′″ piperidyl), 1.69−1.53 (m, 1H, H-4′″ piperidyl), 0.83 (t, $J$ = 7.1 Hz, $OCH_2CH_3$); $^{13}C$ NMR (75 MHz, $CDCl_3$) $\delta$ 167.9 (C═O), 161.0 (C-2 py), 158.4 (C-6 py), 154.0 (C-4 py), 136.6 (C-1′ Ph), 129.5 (C-3′, C-4′, C-5′ Ph), 128.7 (C-2″, C-6″ $CH_2Ph$), 128.4 (C-3″, C-5″ $CH_2Ph$), 128.1 (C-2′, C-6′ Ph), 127.2 (C-4″ $CH_2Ph$), 118.5 (C-3 py), 116.6 (CN), 89.1 (C-5 py), 63.6 ($CH_2Ph$), 61.3 ($OCH_2CH_3$), 53.6 (C-2′″, C-6′″ piperidyl), 47.0 ($NHCH_2$), 36.4 (C-4′″ piperidyl), 30.2 (C-3′″, C-5′″ piperidyl), 24.3 ($CH_3$ pyridyl), 13.7 ($OCH_2CH_3$); MS (ESI) $m/z$: 491$(M+Na)^+$, 469 $(M+H)^+$. Anal. Calcd. for $C_{29}H_{32}N_4O_2$: C, 74.33; H, 6.88; N, 11.96. Found: C, 74.14; H, 7.07; N, 11.83.

*Ethyl 6-(2-(1-Benzylpiperidin-4-yl)ethylamino)-5-cyano-2-methyl-4-phenylnicotinate (**16**).* Following the general procedure, ethyl 6-chloro-5-cyano-2-methyl-4-phenylnicotinate (**22**)[41] (81 mg, 0.29 mmol), triethylamine (0.40 mL, 2.87 mmol), 2-(1-benzylpiperidin-4-yl)ethanamine (**25**)[36] (71 mg, 0.33 mmol), in acetonitrile (10 mL), after 80 h, followed by flash chromatography (*n*-hexane/ethyl acetate 70%), afforded product **16** (69.8 mg, 54%): mp 108−10 °C; IR (KBr) $\nu_{max}$ 3403, 3061, 2925, 2856, 2798, 2752, 2213, 1724, 1577, 1520, 1494 $cm^{-1}$; $^1H$ NMR (400 MHz, $CDCl_3$) $\delta$ 7.64−7.17 (m, 10H, aromatic), 5.34 (t, $J$ = 5.4 Hz, 1H, N−H), 3.92 (q, $J$ = 7.1 Hz, 2H, $OCH_2CH_3$), 3.69−3.57 (m, 2H, $CH_2NH$), 3.50 (s, 2H, $CH_2Ph$), 2.90 (d, $J$ = 11.8 Hz, 2H, H-2′″, H-6′″ piperidyl), 2.52 (s, 3H, $CH_3$ py), 1.96 (t, $J$ = 11.1 Hz, 2H, H-3′″, H-5′″ piperidyl), 1.74 (d, $J$ = 9.4 Hz, 2H,H-3′″, H-5′″ piperidyl), 1.59 (dd, $J$ = 14.0, 6.5 Hz, 1H, H-4′″ piperidyl), 1.34 (dd, $J$ = 16.8, 5.2 Hz, 2H, $CH_2CH_2NH$), 0.83 (t, $J$ = 7.1 Hz, 3H, $OCH_2CH_3$); $^{13}C$ NMR (101 MHz, $CDCl_3$) $\delta$ 167.9 (C═O), 161.0 (C-2 py), 158.2 (C-6 py), 154.0 (C-4 py), 136.6 (C-1′ Ph), 129.5 (C-3′, C-5′ Ph), 129.4 (C-4′ Ph), 128.7 (C-2″, C-6″ $CH_2Ph$), 128.4 (C-3″, C-5 ‘’ $CH_2Ph$),128.1 (C-2′, C-6′ Ph), 127.2 (C-4″ $CH_2Ph$), 118.4 (C-3 py), 116.7 (CN), 89.1 (C-5 py), 63.7 ($CH_2Ph$), 61.3 ($OCH_2CH_3$), 54.0 (C-2′″, C-6′″ piperidyl), 39.3 ($NHCH_2$), 36.5 (C-4′″ piperidyl), 33.5 ($NHCH_2CH_2$), 32.4 (C-3′″, C-5′″ piperidyl), 24.3 ($CH_3$ pyridyl), 13.7 ($OCH_2CH_3$); MS (ESI) $m/z$: 531 $(M+K)^+$, 505 $(M+Na)^+$, 483 $(M+H)^+$. Anal. Calcd. for $C_{30}H_{34}N_4O_2$: C, 74.66; H, 7.10; N, 11.61. Found: C, 74.79; H, 6.99; N, 11.80.

*Ethyl 6-(3-(1-Benzylpiperidin-4-yl)propylamino)-5-cyano-2-methyl-4-phenylnicotinate (**17**).* Following the general procedure, ethyl 6-chloro-5-cyano-2-methyl-4-phenylnicotinate (**22**)[41] (102 mg, 0.34 mmol), triethylamine (0.50 mL, 3.59 mmol), 3-(1-benzylpiperidin-4-yl)propan-1-amine (**26**)[43] (111 mg, 0.48 mmol), in THF/EtOH 3:1 (*v/v*) (13 mL), after 45.5 h, followed by flash chromatography (*n*-hexane/ethyl acetate 30−40%), afforded compound **17** as a brown oil (129 mg, 77%): IR $\nu_{max}$ 3369, 3082, 3028, 2926, 2846, 2800, 2758, 2214, 1716, 1575, 1558, 1516, 1495, 1455, 1366 $cm^{-1}$; $^1H$ NMR (400 MHz, $CDCl_3$) $\delta$ 7.64−7.18 (m, 10 H, aryl groups), 5.39 (t, $J$ = 5.5 Hz, 1H, N−H), 3.92 (q, $J$ = 7.1 Hz, 2H, $OCH_2CH_3$), 3.62−3.47 (m, 4H, $NHCH_2$ + $CH_2Ph$), 2.89 (d, $J$ = 11.4 Hz, 2H, H-2′″, H-6′″ piperidyl), 2.53 (s, 3H, $CH_3$), 1.95 (t, $J$ = 10.9 Hz, 2H, H-3′″, H-5′″ piperidyl), 1.79−1.43 (m, 4H, $NHCH_2CH_2$ + H-3′″, H-5′″ piperidyl), 1.34−1.24 (m, 5H, $NHCH_2CH_2CH_2$ + H-2′″, H-6′″ piperidyl, H-4′″ piperidyl), 0.83 (t, $J$ = 7.1 Hz, 3H, $OCH_2CH_3$); $^{13}C$ NMR (101 MHz, $CDCl_3$) $\delta$ 167.9 (C═O), 161.0 (C-2 py), 158.2 (C-6 py), 154.0 (C-4 py), 136.6 (C-1′ Ph), 129.5 (C-3′, C-5′ Ph), 129.4 (C-4′ Ph), 128.7 (C-2″, C-6″ $CH_2Ph$), 128.4 (C-3″, C-5″ $CH_2Ph$), 128.1 (C-2′, C-6′ Ph), 127.1 (C-4″ $CH_2Ph$), 118.3 (C-3 py), 116.7 (CN), 89.1 (C-5 py), 63.7 ($CH_2Ph$), 61.3 ($OCH_2CH_3$), 54.1 (C-2′″, C-6′″ piperidyl), 41.9 ($NHCH_2$), 35.6 (C-4′″ piperidyl), 33.9 ($NHCH_2CH_2CH_2$), 32.6 (C-3′″, C-5′″ piperidyl), 27.0 ($NHCH_2CH_2$), 24.3 ($CH_3$ pyridyl), 13.7 ($OCH_2CH_3$); MS (ESI) $m/z$: 519 $(M+Na)^+$, 497 $(M+H)^+$. Anal. Calcd. for $C_{31}H_{36}N_4O_2$: C, 74.97; H, 7.31; N, 11.28. Found: C, 74.98; H, 7.24; N, 10.99.

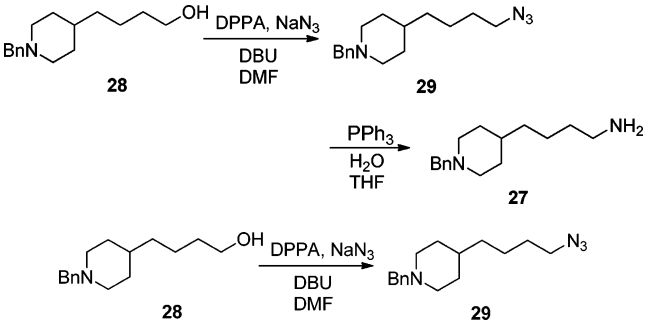


*Synthesis of 4-(4-Azidobutyl)-1-benzylpiperidine (**29**).* Under argon, DPPA (1.97 mL, 9.16 mmol) and 1,8-diazabicyclo[5.4.0]-undec-7-en DBU (1.37 mL, 9.16 mmol) were subsequently added dropwise to a cooled (0 °C) solution of the 4-(1-benzylpiperidin-4-yl)butan-1-ol **28** (0.755 g, 3.053 mmol) in dry DMF (10 mL). After 30 min, $NaN_3$ (0.6 g, 9.16 mmol) was added. After the addition, the cooling bath was removed and the resulting solution was heated at 100 °C for 90 min. After cooling to room temperature, the reaction was diluted by dichloromethane and washed with water, and the organic layer was washed with brine. After drying over sodium sulfate, filtration, and evaporation of the solvent, the crude product was purified by column chromatography (5% of MeOH in $CH_2Cl_2$) to give compound **29** (0.591 g, 71%) as colorless oil; IR (KBr) $\nu$ 2931, 2095, 1591, 1489, 1455, 1316, 1270, 1220, 1193, 1007, 925, $cm^{-1}$; $^1H$ NMR (400 MHz, $CDCl_3$) $\delta$ 7.36−7.23 (m, 5H), 3.49 (s, 2H, $CH_2$−Ph), 3.26 (t, $J$ = 6.9 Hz, 2H, $CH_2$−$N_3$), 2.88 (d, $J$ = 11.0 Hz, 2H), 1.92 (t, $J$ = 10.6 Hz, 2H), 1.66−1.53 (m, 4H). 1.42−1.33 (m, 2H), 1.31−1.16 (m, 5H); $^{13}C$ RMN (100 MHz, $CDCl_3$) $\delta$ 138.4 (C-Ph), 129.1 (2×CH−Ph), 128.0 (2×CH−Ph), 126.8 (CH−Ph), 63.4 ($CH_2$−Ph), 53.8 ($2CH_2$), 51.3 ($CH_2N_3$), 36.0 ($CH_2$−$(CH_2)_3N_3$), 35.5 (CH), 32.2 ($2CH_2$), 29.0 ($CH_2$−$CH_2N_3$), 23.9 ($CH_2$−$(CH_2)_2N_3$); MS (IE) $m/z$ (%): 91 (100) $[PhCH_2]^+$, 195 (43) $[M - Ph]^+$, 202 (8) $[M - (CH_2)_2N_3]^+$, 216 (19) $[M - CH_2N_3]^+$, 230 (9) $[M - N_3]^+$, 271 (10) $[M - H]^+$, 272 (7) $[M]^+$. Anal. Calcd. for $C_{16}H_{24}N_4$: C, 70.55; H, 8.88; N, 20.57. Found: C, 70.36; H, 8.75; N, 20.48

*Synthesis of 4-(1-Benzylpiperidin-4-yl)butan-1-amine (**27**).* Water (0.06 mL, 2.2 mmol) and triphenylphosphine $PPh_3$ (0.144 g, 0.55 mmol) were added to a solution of the 4-(4-azidobutyl)-1-benzylpiperidine **29** (0.1 g, 0.367 mmol) in dry THF (1.5 mL). The reaction mixture was heated at reflux for 2h and 30 min. After completion, the solvent was evaporated and the residue was purified by column chromatography using $CH_2Cl_2$/MeOH (100/20) then $CH_2Cl_2$/MeOH/TEA (100/20/1) to give compound **27** (0.089 g, 98%) as colorless oil; IR (KBr) $\nu$ 2798, 1574, 1493, 1454, 1393, 1341, 736, 698; $^1H$ NMR (400 MHz, $CDCl_3$) $\delta$ 7.32−7.21 (m, 5H), 3.47 (s,

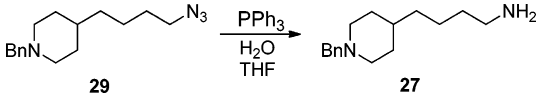



dx.doi.org/10.1021/cn300178k | ACS Chem. Neurosci. 2013, 4, 547−565

2H, $CH_2$−Ph), 2.86 (d, $J$ = 11.2 Hz, 2H), 2.67 (t, $J$ = 5.9 Hz, 2H, $CH_2NH_2$), 2.08 (brs, 2H, $NH_2$), 1.96−1.86 (m, 2H), 1.64- 1.61 (m, 2H), 1.467−1.37 (m, 2H, $CH_2$−$CH_2NH_2$), 1.33−1.20 (m, 7H); $^{13}$C NMR (100 MHz, $CDCl_3$) $\delta$ 138.3 (C−Ph), 129.1 (2×CH−Ph), 128.0 (2×CH−Ph), 126.7 (CH−Ph), 63.4 ($CH_2$−Ph), 53.8 (2C, $2CH_2$), 41.8 ($CH_2NH$), 36.3 ($CH_2$−$(CH_2)_3NH$), 35.5 (CH), 33.34 ($CH_2$−$CH_2NH$), 32.2 (2C, $2CH_2$), 23.9 ($CH_2$−$(CH_2)_2NH$); MS (IE) $m/z$ (%): 91 (100) $[PhCH_2]^+$, 155 (60) $[M - Bn]^+$, 202 (7) $[M - CH_2CH_2NH_2]^+$, 216 (10) $[M - CH_2NH_2]^+$, 245 (9) $[M - H]^+$, 246 (8) $[M]^+$. HRMS (ESI): Calcd for $C_{16}H_{27}N_2$ ($[M+H]^+$): 247.2174. Found: 247.2161.

*Ethyl 6-(4-(1-Benzylpiperidin-4-yl)butylamino)-5-cyano-2-methyl-4-phenylnicotinate (**18**).* Following the general procedure, ethyl 6-chloro-5-cyano-2-methyl-4-phenylnicotinate (**22**)[41] (96 mg, 0.32 mmol), triethylamine (0.45 mL, 3.23 mmol), 4-(1-benzylpiperidin-4-yl)butan-1-amine (**27**) (93 mg, 0.38 mmol), in THF/EtOH 3:1 (v/v) (13 mL), after 50 h, followed by flash chromatography (*n*-hexane/ethyl acetate 20−50%), afforded compound **18** (99.1 mg, 61%): mp 87−9 °C; IR (KBr) $\nu_{max}$ 3429, 3346, 3060, 3028, 2930, 2855, 2803, 2758, 2219, 1713, 1584, 1558, 1514, 1456, 1365, 1273 cm$^{-1}$; $^1$H NMR (400 MHz, $CDCl_3$) $\delta$ 7.60−7.11 (m, 10H, aromatic), 5.35 (t, $J$ = 5.4 Hz, 1H, NH), 3.90 (q, $J$ = 7.1 Hz, 2H, $OCH_2CH_3$), 3.61−3.39 (m, 4H, $NHCH_2$ + $CH_2$Ph), 2.86 (d, $J$ = 10.8 Hz, 2H, H-2′″, H-6′″ piperidyl), 2.51 (s, 3H, $CH_3$), 1.92 (t, $J$ = 10.3 Hz, 2H, H-3′″, H-5′″ piperidyl), 1.72−1.52 (m, 4H, $NHCH_2CH_2$ + H-3′″, H-5′″ piperidyl), 1.46−1.12 (m, 7H, $NHCH_2CH_2CH_2$ + $NHCH_2$ $CH_2CH_2CH_2$ + H-2′″, H-6′″ piperidyl + H-4′″ piperidyl), 0.82 (t, $J$ = 7.1 Hz, 3H, $OCH_2CH_3$); $^{13}$C NMR (101 MHz, $CDCl_3$) $\delta$ 167.9 (C═O), 161.1 (C-2 py), 158.2 (C-6 py), 154.0 (C-4 py), 136.6 (C-1′ Ph), 129.5 (C-3′, C-5′ Ph), 129.4 (C-4′ Ph), 128.7 (C-2″, C-6″ $CH_2$Ph), 128.4 (C-3″, C-5″ $CH_2$Ph), 128.1 (C-2′, C-6′ Ph), 127.1 (C-4″ $CH_2$Ph), 118.3 (C-3 py), 116.7 (CN), 89.1 (C-5 py), 63.7 ($CH_2$Ph), 61.3 ($OCH_2CH_3$), 54.1 (C-2′″, C-6′″ piperidyl), 41.7 ($NHCH_2$), 36.4 (C-4′″ piperidyl), 35.9 ($NHCH_2CH_2$), 32.5 (C-3′″, C-5′″ piperidyl), 29.9 ($NHCH_2CH_2CH_2$ + $NHCH_2CH_2CH_2CH_2$), 24.3 ($CH_3$ pyridyl), 13.7 ($OCH_2CH_3$); MS (ESI) $m/z$: 533 $(M+Na)^+$, 511 $(M+H)^+$; Anal. Calcd. for $C_{32}H_{38}N_4O_2$: C, 75.26; H, 7.50; N, 10.97. Found: C, 75.45; H, 7.73; N, 10.68.

*(E)-4-(1-Benzylpiperidin-4-yl)but-3-en-2-one (**32**).* A mixture of $K_2CO_3$ (4.14 g, 30 mmol) and diethyl (2-oxopropyl)phosphonate (2 mL, 10 mmol) in dry THF (30 mL) was stirred at rt for 15 min and refluxed for 20 min. After cooling, 1-benzylpiperidine-4-carbaldehyde (**31**)[47] (2.03 g, 10 mmol) in 20 mL of THF was added, and the mixture was heated under reflux for 3 h. After cooling, a 10% $K_2CO_3$ solution (100 mL) was added, and the mixture was extracted with $CH_2Cl_2$. The organic phase was dried over $Na_2SO_4$ and evaporated under reduce pressure. The crude product was purified by flash chromatography (hexane/EtOAc, 7/3, v/v) to give compound 32 (2.18 g, 90%) as a as brown oil; $R_f$ = 0.3 (hexane/AcOEt, 1/1, v/v); IR (KBr) $\nu$ 2934, 1676, 1494, 1365, 1258, 979 cm$^{-1}$; $^1$H NMR (400 MHz, $CDCl_3$) $\delta$ 7.44−7.10 (m, 5H, Ph), 6.73 (dd, $J$ = 16.1, 6.7 Hz, 1H), 6.04 (dd, $J$ = 16.1, 1.2 Hz, 1H), 3.51 (s, 2H), 2.92 (d, $J$ = 11.7 Hz, 2H), 2.23 (s, 3H), 2.15 (d, $J$ = 7.0 Hz, 1H), 2.02 (td, $J$ = 11.7, 2.2 Hz, 2H), 1.72 (d, $J$ = 12.9 Hz, 2H), 1.52 (td, $J$ = 12.0, 3.3 Hz, 2H); $^{13}$C NMR (101 MHz, $CDCl_3$) $\delta$ 198.81 (CO), 151.74, 138.08 (C1′), 129.31 (CH), 129.10 (2C, CH(Ph)), 128.14 (2C, CH(Ph)), 126.98 (C4′, CH(Ph)), 63.24 ($PhCH_2$), 53.08 ($2CH_2$), 38.76 (CH), 30.90 ($2CH_2$), 26.89 ($CH_3$); MS (EI) $m/z$: 243 (M)+, 228 (M−$CH_3$)+, 91 ($PhCH_3$)+, MS (ES) $m/z$ [M+1]+ 244.3, [M+Na]+ 266.6. Anal. Calcd. for $C_{16}H_{21}NO$: C, 78.97; H, 8.70; N, 5.76. Found: C, 78.75; H, 8.91; N, 5.95.

*4-(1-Benzylpiperidin-4-yl)butan-2-one (**33**).* To a solution of (*E*)-4-(1-benzylpiperidin-4-yl)but-3-en-2-one (**32**) (1.5 g, 6.17 mmol) in EtOH (20 mL) was added $PtO_2$ (150 mg, 10%), and the mixture was hydrogenated for 4 h at room temperature. The reaction was filtered over Celite and washed with EtOAc. The organic layer was concentrated to give compound **33** (1.52 g 99%) as brown oil; $R_f$ = 0.6 (hexane/AcOEt, 8/2, v/v); IR (KBr) $\nu$ 3027, 2924, 2800, 1716, 1452, 1365, 740, 699 cm$^{-1}$; $^1$H NMR (400 MHz, $CDCl_3$) $\delta$ 7.44−7.12 (m, 5H, PH), 3.48 (s, 2H, $PhCH_2$), 2.87 (d, $J$ = 11.8 Hz, 2H, $CH_2$), 2.46−2.39 (m, 2H, $CH_2$), 2.12 (s, 3H, $CH_3$), 1.92 (t, $J$ = 11.3 Hz, 2H, $CH_2$), 1.70 (m, 2H, $CH_2$), 1.56 (m, 2H, $CH_2$), 1.44 (m, 3H, CH +$CH_2$); $^{13}$C NMR (101 MHz, $CDCl_3$) $\delta$ 209.10 (CO), 138.15 (C1′), 129.1 (2C, CH(Ph)), 128.0 (2C, CH(Ph)), 126.8 (C4′, CH(Ph)), 63.3 ($PhCH_2$), 53.6 ($2CH_2$), 41.0 ($CH_2$), 35.1 (CH), 31.9 ($2CH_2$), 30.1 ($CH_2$), 29.7 ($CH_3$); MS (ES) $m/z$ $[M+1]^+$ 246.3. Anal. Calcd. for $C_{16}H_{23}NO$: C, 78.32; H, 9.45; N, 5.71. Found: C, 78.15; H, 9.64; N, 5.66.

*6-((1-Benzylpiperidin-4-ylidene)methyl)-2-ethoxy-7-methyl-4-phenyl-1,8-naphthyridine −3-carbonitrile (**19**).* A solution of KOH 10% in EtOH (50 mg in 0.62 mL) was added dropwise to a solution of 6-amino-2-ethoxy-5-formyl-4-phenylnicotinonitrile (**30**)[47] (156 mg, 0.56 mmol, 1 equiv) and (*E*)-4-(1-benzylpiperidin-4-yl)but-3-en-2-one (**32**) (142 mg, 0.56 mmol, 1 equiv) in 10 mL of EtOH. The reaction mixture was heated for 30 min. The reaction was concentrated, washed with water, and extracted with $CH_2Cl_2$. The organic layer was dried with $Na_2SO_4$ and concentrated to give the desired compound **19** (135 mg, 49%): mp 146−147 °C; IR(KBr) $\nu$ 2975, 2787, 2228, 1587, 1572, 1453, 1332 cm$^{-1}$. $^1$H NMR (400 MHz, $CDCl_3$) $\delta$ 7.60−7.53 (m, 3H), 7.52 (s, 1H, H5), 7.44−7.38 (m, 2H), 7.34−7.22 (m, 5H), 6.19 (s, 1H, H4″a), 4.75 (q, $J$ = 7.1 Hz, 2H, $OCH_2$), 3.49 (s, 2H), 2.70 (s, 3H), 2.52 (t, $J$ = 5.4 Hz, 2H), 2.39 (t, $J$ = 5.4 Hz, 2H), 2.32 (t, $J$ = 5.5 Hz, 2H), 2.19 (t, $J$ = 5.5 Hz, 2H), 1.51 (t, $J$ = 7.1 Hz, 3H); $^{13}$C NMR ($CDCl_3$, 100 MHz) $\delta$ 165.3 (C7), 162.3 (C2), 158.1 (C4), 154.3 (C8a), 143.2 (C4″), 138.3 (C5), 135.8 (C4a), 133.4, 130.6, 130.3, 129.4, 129.3, 129.1, 128.4, 127.3 (10 CH(Ph)), 119.2 (C4″a), 116.0 (C6), 114.8 (CN), 98.3 (C3), 64.2 ($NCH_2C_6H_5$), 63.0 ($OCH_2CH_3$), 55.1 ($C2''H_2$), 54.3 ($C6''H_2$), 36.4 ($C3''H_2$), 29.4 ($C5''H_2$), 24.4 [$C(7)CH_3$], 14.6 ($OCH_2CH_3$). Anal. Calcd. for $C_{31}H_{30}N_4O$: C, 78.45; H, 6.37; N,11.81. Found: C, 78.28; H, 6.41; N, 11.87.

*7-(2-(1-Benzylpiperidin-4-yl)ethyl)-2-ethoxy-4-phenyl-1,8-naphthyridine-3-carbonitrile (20) and 6-((1-Benzylpiperidin-4-yl)methyl)-2-ethoxy-7-methyl-4-phenyl-1,8-naphthyridine-3-carbonitrile (**21**).* To a solution of 6-amino-2-ethoxy-5-formyl-4-phenylnicotinonitrile **30**[47] (72 mg, 0.27 mmol) and 4-(1-benzylpiperidin-4-yl)butan-2-one (**33**) (53 mg, 0.24 mmol, 0.9 equiv) in a mixture of $CH_2Cl_2$/MeOH (2/6 mL, v/v) was added dropwise pyrrolidine (6 $\mu$L, 0.07 mmol, 0.25 equiv). The reaction was stirred at room temperature for 28 h. After completion, the solvent was evaporated off, and the residue was purified by column chromatography (from 1 to 20% of $CH_2Cl_2$ in methanol) to give compounds **20** and **21**. **20**: White solid (48 mg, 42%): $R_f$ = 0.17 ($CH_2C_2$/MeOH, 9.5/0.5, v/v); mp 119−121 °C; IR (KBr) $\nu$ 2919, 2802, 2762, 2228, 1588, 1333, 1024 cm$^{-1}$; $^1$H NMR ($CDCl_3$, 300 MHz) $\delta$ 7.85 (d, $J$ = 8.4 Hz, 1H, CH), 7.59 (m, 3H, Ph), 7.43 (m, 2H, Ph), 7.28 (m, 5H, Ph), 7.22 (d, 1H, $J$ = 8.4 Hz, CH), 4.79 (q, 2H, $J$ = 7.09 Hz, $OCH_2CH_3$), 3.52 (s, 2H, $CH_2$), 3.01 (m, 2H, $C^{6'}H_2$), 2.92 (m, 2H, $C^{8'}H$+$C^{2'}H$), 1.97 (m, 2H, $C^{2'}H$+$C^{8'}H$), 1.74 (m, 4H, $C^{5'}H_2$ +($C^{3'}H$ + $C^{7'}H$)), 1.53 (t, 3H, $J$ = 7.09 Hz, $OCH_2CH_3$), 1.36 (m, 3H, $C^{4'}H$ +($C^{3'}H$ + $C^{7'}H$)); $^{13}$C NMR ($CDCl_3$, 75 MHz) $\delta$ 169.9 (C7), 162.7 (C2), 158.5 (C8a), 155.9 (C4), 138.2 (C′4), 136.7 (C5), 133.4 (C′″1), 130.3 (CH(Ph)), 129.6 (CH(Ph)), 129.58 (2CH(Ph)), 129.51 (2CH(Ph)), 129.2 (2CH(Ph)), 128.4 (CH(Ph)), 127.3 (CH(Ph)), 121.1 (C6), 116.1 (C4a), 114.7 (CN), 98.5 (C3), 64.36 ($OCH_2$), 64.32 (C1″, $CH_2$), 53.8 (C5′, C6′, $2CH_2$), 37.1 ($CH_2$), 36.8 ($CH_2$), 36.0 ($C^{4'}H$), 32.2 ($2CH_2$), 14.6 ($CH_3$); MS (ES) $m/z$ $[M+1]^+$ 477.5, $[2M+Na]^+$ 975.9. Anal. Calcd. for $C_{31}H_{32}N_4O$: C, 78.12; H, 6.17; N, 11.76. Found: C, 77.99; H, 6.58; N, 11.53. **21**: Yellow solid (23 mg, 20%): $R_f$ = 0.25 ($CH_2C_2$/MeOH, 9.5/0.5, v/v); mp 129−132 °C; IR(KBr) $\nu$ 2924, 2227, 1587, 1331, 1023 cm$^{-1}$; $^1$H NMR ($CDCl_3$, 400 MHz) $\delta$ 7.60 (m, 3H, Ph), 7.53 (s, 1H, CH), 7.43 (m, 2H, Ph), 7.28 (m, 5H, Ph), 4.75 (q, $J$ = 7.1 Hz, 2H, $OCH_2CH_3$), 3.48 (s, 2H, $CH_2Ph$), 2.87 (d, $J$ = 11.2 Hz, 2H, $CH_2$), 2.76 (s, 3H, $CH_3$), 2.60 (d, $J$ = 6.9 Hz, 2H, $CH_2$), 1.88 (t, $J$ = 11.2 Hz, 2H, $CH_2$), 1.52 (t, $J$ = 7.1 Hz, 3H, $OCH_2CH_3$), 0.88 (t, $J$ = 6.9 Hz, 1H, CH); $^{13}$C NMR (101 MHz, $CDCl_3$) $\delta$ 165.2 (C7), 162.3 (C2), 158.0 (C4), 154.2 (C8a), 136.1 (C5), 133.4 (C6), 132.6 (C1′), 130.3 (C1″), 129.4 (3C(Ph)), 129.2 (2C(Ph)), 128.4 (2C(Ph)), 127.2 (C4″), 116.2 (C4a), 114.8 (CN), 98.4 (C3), 64.2 ($CH_2$), 63.4 ($CH_2$), 53.7 ($CH_2$), 39.8 ($CH_2$), 36.4 ($CH_2$), 32.2 ($CH_2$), 31.7 (CH), 23.8 ($CH_3$), 22.8 ($CH_2$), 14.6 ($CH_3$). MS (ES) $m/z$ $[M+1]^+$ 477.5, $[M+Na]^+$ 499.5,


dx.doi.org/10.1021/cn300178k | ACS Chem. Neurosci. 2013, 4, 547−565

$[2M+Na]^+$ 975.9. Anal. Calcd. for $C_{31}H_{32}N_4O$: C, 78.12; H, 6.17; N, 11.76. Found: C, 77.94; H, 6.58; N, 11.49.

**Pharmacology.** *Inhibition of EeAChE and eqBuChE.* To assess the inhibitory activity of ChEs, the spectrophotometric method of Ellman[51] was followed, using purified AChE from *Electrophorus electricus* (Type V-S, Sigma) or BuChE from horse serum (lyophilized powder) (Sigma Aldrich, Madrid, Spain). The reaction took place in a final volume of 3 mL of a phosphate-buffered solution (0.1 M) at pH 8, containing 0.035 U of AChE or 0.05 U of BuChE and 0.35 mM 5,5′-dithiobis-2-nitrobenzoic acid (DTNB, Sigma-Aldrich, Madrid, Spain). Inhibition curves were made by preincubating this mixture with at least nine concentrations of each compound for 10 min. A sample with no compound was always present to determine the percent of enzyme activity. After this preincubation period, acetylthiocholine iodide (0.35 mM) or butyrylthiocholine iodide (0.5 mM) (Sigma-Aldrich, Madrid, Spain) was added, allowing 15 min of incubation, where the DTNB produces the yellow anion 5-thio-2-nitrobenzoic acid along with the enzymatic degradation of acetylthiocholine iodide or butyrylthiocholine iodide. Changes in absorbance were detected at 405 nm in a spectrophotometric plate reader (FluoStar OPTIMA, BMG Labtech). Compounds inhibiting AChE or BuChE activity would reduce the color generation; thus, $IC_{50}$ values were calculated as the concentration of compound that produces 50% of the AChE activity inhibition. Data are expressed as means ± SEM of at least three different experiments in quadruplicate.

*Kinetic Analysis of the AChE Inhibition by Compounds* ***16*** *and* ***18****.* To obtain estimates of the inhibition constant $K_i$, reciprocal plots of $1/V$ versus $1/[S]$ were constructed at different concentrations of the substrate acetylthiocholine (0.1−0.8 mM) by using Ellman's method.[51] Experiments were performed in a transparent 48-well plate in a final volume of 1 mL of a phosphate-buffered solution (0.1 M) at pH 8, containing each well 400 μL of 0.875 mM DTNB solution, 1 μL of DMSO (control) or inhibitor solution to give desired final concentration, and 14 μL of EeAChE (3.6 U/mL) at 30 °C to give a final concentration of 0.05 U/mL. Reaction was initiated by adding acetylthiocholine at the concentrations proposed (0.1−0.8 mM). Progress curves were monitored at 410 nm over 2 min in a fluorescence plate reader Fluostar Optima (BMG-technologies, Germany), absorbance ready. Progress curves were characterized by a linear steady-state turnover of the substrate, and values of a linear regression were fitted according to Lineweaver−Burk replots using Origin software. The plots were assessed by a weighted least-squares analysis. Determination of the Michaelis constant for the substrate acetylthiocholine was done at five different concentrations (0.1−0.8 mM) to give $K_M$ = 0.48 mM and $V_{max}$ = 0.37 $min^{-1}$. Slopes of the reciprocal plots were then plotted against the concentration of compounds **16** and **18** (range 0−0.3 μM) to evaluate $K_i$ data. Data analysis was performed with Origin Pro 7.5 software (Origin Lab Corp.).

*Inhibition of Human AChE and BuChE.* To assess the inhibitory activity of both ChEs, the spectrophotometric method of Ellman was followed.[51] The assay solution consisted of 0.1 M phosphate buffer pH 8, 400 μM 5,5′-dithiobis(2-nitrobenzoic acid) (DTNB, Ellman's reagent), 0.05 U/mL hAChE (human recombinant acetylcholinesterase, Sigma Chemical Co.) or 0.024 U/mL hBuChE (butyrylcholinesterase from human serum, Sigma Chemical Co.), and 800 μM acetylthiocholine iodide, or 500 μM butyrylthiocholine as the substrate of the enzymatic reaction, respectively. The compounds tested were added to the assay solution and preincubated with the enzyme for 5 min at 30 °C. After that period, the substrate was added. The absorbance changes at 412 nm were recorded for 5 min with a UV/vis microplate spectrophotometer, Multiskan Spectrum, Thermo-Electron Co. The reaction rates were compared and the inhibition percent due to the presence of test compound was calculated. The $IC_{50}$ is defined as the concentration of each compound that reduces at 50% the enzymatic activity without any inhibitor.

*Neuronal Cell Line Cultures.* The human neuroblastoma cell line SH-SY5Y (American Type Culture Collection, Dulbecco's modified Eagle's medium nutrient mixture F-12 (DMEM-F12), at passages between 3 and 10 after defreezing, was maintained in DMEM F-12 and supplemented with 10% fetal calf serum (heat-inactivated; Invitrogen, Barcelona, Spain), 1 μM glutamine, 50 U/mL penicillin, and 50 μg/mL streptomycin (Invitrogen, Barcelona, Spain). Cultures were seeded into flasks containing supplemented medium and maintained at 37 °C in 5% $CO_2$, humidified air. Stock cultures were passaged 1:4 twice weekly. For assays, SH-SY5Y cells were subcultured in 24-well plates at a seeding density of $2 \times 10^5$ cells per well.

*Cell Viability (MTT Assay).* The MTT (3-[4,5-dimethylthiazol-2-yl]-2,5-diphenyltetrazolium bromide) (SIGMA) is reduced to formazan by metabolic active cells, and therefore, this conversion is directly related to the amount of viable cells. Briefly, MTT was dissolved in Krebs medium, containing (in mM): NaCl 132, KCl 4, $CaCl_2$ 1, $MgCl_2$ 1.4, $H_3PO_4$ 1.2, glucose 6, and HEPES-Na 10 (pH = 7.4), to a concentration of 5 mg/mL and then added to the neuronal culture medium for 2 h at 37 °C. After this incubation, the medium was removed and the blue formazan crystals formed were dissolved in DMSO[56] and quantified by measuring absorbance at 570 nm in a Molecular Devices SpectraMax Plus 384 plate reader. Results were expressed as a percentage of the absorbance in control cells.

*Aβ Peptides and Cell Treatment.* The $A\beta_{1-42}$ peptide (American Peptide, Sunnyvale, CA) was dissolved in water at a concentration of 2 mg/mL. Aliquots of this solution were kept frozen until added to cell cultures. This $A\beta_{1-42}$ solution contains mainly oligomeric forms of the peptide. The SH-SY5Y cells (before confluence) were treated with the phenoxyalkylamino-4-phenylnicotinates (2−7), phenoxyalkoxybenzylidenemalononitriles (12,13), pyridonepezils (14−18), and pyrazolo-[3,4-*b*]quinolines (35−37) (dissolved in DMSO) at the concentrations indicated in the figure legends, alone or in combination with $A\beta_{1-42}$ at a concentration of 2 μM for 24 h.

*Measurement of AChE Activity.* Neuronal cells were lysed in 15 mM Tris (pH 7.4), on ice, and AChE activity was measured using a spectrophotometric method.[51,57] Acetylthiocholine iodide (SIGMA) was used as substrate, at a concentration of 0.5 mM. Ethopropasine−HCl (0.1 mM) was used to inhibit nonspecific esterases. The activity of AChE was measured spectrophotometrically at 414 nm and expressed as μmol of acetylthiocholine iodide hydrolyzed/min/mg protein. Several assays were performed simultaneously using a Molecular Devices SpectraMax Plus 384 plate reader. The protein content of samples was determined by using the Bio-Rad protein dye assay and a standard curve with a known amount of bovine serum albumin.

*Measurement of Propidium Iodide Displacement.* A solution of AChE from bovine erythrocytes (type XII-S, Sigma Aldrich, Madrid, Spain) at the concentration of 5 μM in 0.1 mM Tris buffer, pH 8, was used. Aliquots of the compound to get a final concentration of 100 μM were added, and the solutions were kept at room temperature for at least 20 h. BW284C51 (Sigma Aldrich, Madrid, Spain) was used as standard.[70] After that time, the samples were incubated for 15 min with propidium iodide (Invitrogen, Eugene, OR) at 20 μM and the fluorescence was measured in a fluorescence microplate reader (FLUOstar Optima, BMG, Germany). Wavelengths of excitation and emission were 485 and 620 nm, respectively.

*Cytosolic $Ca^{2+}$ Measurements.* $Ca^{2+}$ transients in SHSY5Y neuronal cells were measured using the fluorescent probe Fura-2/AM, performed as previously described[71] with some modifications. In brief, neuronal cells previously exposed to compounds (or not, control cells) in the presence or absence of $A\beta_{1-42}$ were washed in Krebs medium, containing (in mM) NaCl 132, KCl 4, $CaCl_2$ 1, $MgCl_2$ 1.4, glucose 6, and HEPES-Na 10 (pH = 7.4) supplemented with 10 mM $NaHCO_3$ and 0.05 mM EGTA. The cells were then loaded with Fura-2/AM (5 μM) in Krebs medium supplemented with 0.2% (w/v) pluronic acid for 40 min, at 37 °C in the dark. Afterward, the cells were washed and then incubated in Fura-2/AM-free Krebs medium for 15 min, at 37 °C in the dark, to ensure the complete hydrolysis of the dye (reagents from SIGMA). Fluorescence was monitored using a microplate reader (SpectraMax reader Gemini EM, Molecular Devices) at 510 nm emission and double excitation at 340 and 380 nm.

*Molecular Docking into AChE and BuChE.* Compounds **16** and **18** were assembled as hydrochloride within Discovery Studio, version 2.1,

software package, using standard bond lengths and bond angles. With the CHARMm force field[72] and partial atomic charges, the molecular geometries of **16** and **18** were energy-minimized using the adopted-based Newton−Raphson algorithm. Structures were considered fully optimized when the energy changes between iterations were less than 0.01 kcal/mol.[73]

*Molecular Docking of Compounds **16** and **18** into EeAChE and hAChE.* The coordinates of EeAChE (PDB ID: 1C2B) and *h*AChE (PDB ID: 1B41) were obtained from the Protein Data Bank (PDB). For docking studies, initial protein was prepared by removing all water molecules, heteroatoms, any cocrystallized solvent, and the ligand. Proper bonds, bond orders, hybridization, and charges were assigned using protein model tool in Discovery Studio, version 2.1, software package. CHARMm force field was applied using the receptor−ligand interactions tool in Discovery Studio, version 2.1, software package. Docking calculations were performed with the program Autodock Vina.[61] AutoDockTools (ADT; version 1.5.4) was used to add hydrogens and partial charges for proteins and ligands using Gasteiger charges. Flexible torsions in the ligands were assigned with the AutoTors module, and the acyclic dihedral angles were allowed to rotate freely. Trp286, Tyr124, Tyr337, Tyr72, Asp74, Thr75, Trp86, and Tyr341 receptor residues were selected to be flexible during docking simulation using the AutoTors module. The box center was defined and the docking box was displayed using ADT. The docking procedure was applied to the whole protein target, without imposing the binding site ("blind docking"). A grid box of 60 × 60 × 72 with grid points separated 1 Å was positioned at the middle of the proteins ($x$ = 21.5911; $y$ = 87.752; $z$ = 23.591) for the *Ee*AChE and ($x$ = 116.546; $y$ = 110.33; $z$ = −134.181) for the hAChE. Default parameters were used except num_modes, which was set to 40. The AutoDock Vina docking procedure used was previously validated.[62]

*Molecular Docking of Inhibitors **16** and **18** into eqBuChE and hBuChE.* The horse BuChE model has been retrieved from the SWISS-MODEL Repository. This is a database of annotated three-dimensional comparative protein structure models generated by the fully automated homology-modeling pipeline SWISS-MODEL. A putative three-dimensional structure of eqBuChE has been created based on the crystal structure of *h*BuChE (PDB ID: 2PM8); these two enzymes exhibited 89% sequence identity. The coordinates of hBuChE were obtained from the Protein Data Bank (PDB ID: 2P0I). Proper bonds, bond orders, hybridization, and charges were assigned using protein model tool in Discovery Studio, version 2.1, software package. CHARMm force field was applied using the receptor−ligand interactions tool in Discovery Studio. Docking calculations were performed following the same protocol described before for hAChE. All dockings were performed as blind dockings where a cube of 75 Å with grid points separated 1 Å was positioned at the middle of the proteins ($x$ = 29.885; $y$ = −54.992; $z$ = 58.141) for EqBChE and ($x$ = 137.985; $y$ = 122.725; $z$ = 38.78) for hAChE. Default parameters were used except num_modes, which was set to 40. The lowest docking-energy conformation was considered as the most stable orientation. Finally, the docking results generated were directly loaded into Discovery Studio, version 2.1.

## ■ ASSOCIATED CONTENT

### Ⓢ Supporting Information

Additional synthesis details as described in the text. This material is available free of charge via the Internet at http://pubs.acs.org.

## ■ AUTHOR INFORMATION

### Corresponding Author

*(P.A.) Fax: + 351-239 853 409. E-mail: pagostinho@fmed.uc.pt. (J.M.-C.) Fax: +34-91-5644853. E-mail: iqoc21@iqog.csic.es. (M.C.C.) Fax: +351-21-7946470. E-mail: mcdamaso@ff.ul.pt.

### Author Contributions

D.S. and M.C. have contributed equally to this work. J.M.-C. and M.C.C. are responsible for the supervision and development of the whole project. A.S. supervised the chemical syntheses. D.S. and M.C. carried out chemical syntheses. P.A and P.G. performed the neuronal viability with MTT, the neuroprotection experiments against A$\beta$-toxicity, the impact on the enhancement of AChE activity caused by A$\beta$ peptides, and the effect of compounds in intracellular homeostasis dysregulation. R.L.-C. carried out the propidium iodide displacement assay. C.d.l.R., R.L.-C., E.M., A.S., and L.G.-L. performed the kinetic analysis and the *Ee*ChE and eqBuChE inhibition studies. I.I. and I.M. carried out the molecular modeling analysis. C.P. and M.I.R.-F. carried out the hChE inhibition studies.

### Funding

D.S. thanks FCT, Ministério da Ciência, Tecnologia e Ensino Superior of Portugal for his grant belonging to project PTDC/SAU-NEU/64151/2006. M.C. thanks Instituto de Salud Carlos III (MICINN) for a "Sara Borrell" postdoctoral contract. M.C.C. thanks FCT for funding (Project PTDC/SAU-NEU/64151/2006). J.M.-C. thanks MICINN (SAF2006-08764-C02-01; SAF2009-07271; SAF2012-33304) financial support. D.S. and E.M. thank COST Action D34. M.I.R.-F. thanks grants from MINECO (SAF2009-13015 and SAF2012-31035) and "Fundación de Investigación Médica Mutua Madrileña Automovilística" (AP103952012). This work was partly supported by grant CP10/00531, Miguel Servet Program (ISCarlos III).

### Notes

The authors declare no competing financial interest.

## ■ ABBREVIATIONS

A$\beta$, amyloid beta peptide; AChE, acetylcholinesterase; AChEIs, acetylcholinesterase inhibitors; AD, Alzheimer's disease; APP, amyloid precursor protein; ATCh, acetylthiocholine; CC, catalytic center; ChEs, cholinesterases; ChEIs, cholinesterase inhibitors; DMSO, dimethyl sulfoxide; *Ee*AChE, *Electrophorus electricus* acetylcholinesterase; eqBuChE, horse serum butyrylcholinesterase; hAChE, human recombinant acetylcholinesterase; hBuChE, human serum butyrylcholinesterase; PAS, peripheral anionic site

## ■ REFERENCES

(1) Bertram, L., and Tanzi, R. E. (2008) Thirty years of Alzheimer's disease genetics: the implications of systematic meta-analyses. *Nat. Rev. Neurosci. 9*, 768−778.

(2) Shah, R. S., Lee, H.-G., Xiongwei, Z., Perry, G., Smith, M. A., and Castellani, R. J. (2008) Current approaches in the treatment of Alzheimer's disease. *Biomed. Pharmacother. 62*, 199−207.

(3) Wenk, G. L. (2003) Neuropathologic changes in Alzheimer's disease. *J. Clin. Psychiatry 64*, 7−10.

(4) Terry, A. V., Jr., and Buccafusco, J. J. (2003) The Cholinergic hypothesis of age and Alzheimer's disease-related cognitive deficits: Recent challenges and their implications for novel drug development. *J. Pharmacol. Exp. Ther. 306*, 821−827.

(5) Francis, P. T., Palmer, A. M, Snape, M., and Wilcock, G. K. (1999) The Cholinergic hypothesis of Alzheimer's disease: a review of progress. *J. Neurol. Neurosurg. Psychiatry 66*, 137−147.

(6) Benzi, G., and Moretti, A. (1998) Is there a rationale for the use of acetylcholinesterase inhibitors in the therapy of Alzheimer's disease? *Eur. J. Pharmacol. 346*, 1−13.

(7) Inestrosa, N. C, Alvarez, A., Pérez, C. A., Moreno, R. D., Vicente, M., Linker, C., Casanueva, O. I., Soto, C., and Garrido, J. (1996)

Acetylcholinesterase acceleratyes assembly of amyloid-beta-peptides into Alzheimeŕs fibrils: possible role of the peripheral site of the enzyme. *Neuron 16*, 881−91.
(8) Reyes, A. E., Perez, D. R., Alvarez, A., Garrido, J., Gentry, M. K., Doctor, B. P., and Inestrosa, N. C. (1997) A monoclonal antibody against acetylcholinesterase inhibits the formation of amyloid fibrils induced by the enzyme. *Biochem. Biophys. Res. Commun. 232*, 652−655.
(9) Inestrosa, N. C., Alvarez, A., Godoy, J., Reyes, A., and De Ferrari, G. V. (2000) Acetylcholinesterase-amyloid-beta-peptide interaction and Wnt signaling involvement in Abeta neurotoxicitity. *Acta Neurol. Scand. Suppl. 102*, 53−56.
(10) Mori, F., Lai, C. C., Fusi, F., and Giacobini, E. (1995) Cholinesterase inhibitors increase secretion of APPs in rat brain cortex. *NeuroReport 7*, 633−636.
(11) Giacobini, E. (2003) Cholinesterases: New roles in brain function and in Alzheimeŕs disease. *Neurochem. Res. 28*, 515−522.
(12) Francis, P. T., Nordberg, A., and Arnold, S. E. (2005) A preclinical view of cholinesterase inhibitors in neuroprotection: do they provide more than symptomatic benefits in Alzheimeŕs disease? *Trends Pharmacol. Sci. 26*, 104−111.
(13) Castro, A., and Martinez, A. (2001) Peripheral and dual binding site acetylcholinesterase inhibitors: implications in treatment of Alzheimeŕs disease. *Mini-Rev. Med. Chem. 1*, 267−272.
(14) Pang, Y. P., Quiram, P., Jelaçic, T., Hong, F., and Brimijoin, S. (1996) Highly potent, selective, and low cost bis-tetrahydroaminacrine inhibitors of acetylcholinesterase. Steps toward novel drugs for treating Alzheimer's disease. *J. Biol. Chem. 271*, 23646−23649.
(15) Carlier, P. R., Han, Y. F., Chow, E. S., Li, C. P., Lieu, T. X., Wong, H. S., and Pang, Y. P. (1999) Evaluation of short-tether bis-THA AChE inhibitors. A further test of the dual binding site hypothesis. *Bioorg. Med. Chem. 7*, 351−357.
(16) Mary, A., Renko, D. Z., Guillou, C., and Thal, C. (1998) Potent acetylcholinesterase inhibitors: design, synthesis, and structure-activity relationships of bis-interacting ligands in the galanthamine series. *Bioorg. Med. Chem. 6*, 1835−1850.
(17) Bolognesi, M. L., Andrisano, V., Bartolini, M., Banzi, R., and Melchiorre, C. (2005) Propidium-based polyamine ligands as potent inhibitors of acetylcholinesterase and acetylcholinesterase-induced amyloid-$\beta$ aggregation. *J. Med. Chem. 48*, 24−27.
(18) Davis, K. L., and Powchick, P. (1995) Tacrine. *Lancet 345*, 625−630.
(19) Spencer, C. M., and Noble, S. (1998) Rivastigmine. A review of its use in Alzheimeŕs disease. *Drugs Aging 13*, 391−400.
(20) Barner, E. L., and Gray, S. L. (1998) Donepezil use in Alzheimer disease. *Ann. Pharmacother. 32*, 70−77.
(21) Sramek, J. J., Frackiewicz, E. J., and Cutler, N. R. (2000) Review of the acetylcholinesterase inhibitor galanthamine. *Expert Opin. Invest. Drugs 9*, 2393−2402.
(22) Li, W., Mak, M., Jiang, H., Wang, Q., Pang, Y., Chen, K., and Han, Y. (2009) Novel anti-Alzheimer's dimer Bis(7)-cognitin: cellular and molecular mechanisms of neuroprotection through multiple targets. *Neurotherapeutics 6*, 187−201.
(23) Han, Y. F., Li, C. P.-L., Chow, E., Wang, H., Pang, Y. P., and Carlier, P. R. (1999) Dual-site binding of bivalent 4-aminopyridine- and 4-aminoquinoline-based AChE inhibitors: contribution of the hydrophobic alkylene tether to monomer and dimer affinities. *Bioorg. Med. Chem. 7*, 2569−2575.
(24) Camps, P., Formosa, X., Galdeano, C., Gómez, T., Muñoz-Torrero, D., Scarpellini, M., Viayna, E., Badia, A., Clos, M. V., Camins, A., Pallás, M., Bartolini, M., Mancini, F., Andrisano, V., Estelrich, J., Lizondo, M., Bidon-Chanal, A., and Luque, F. J. (2008) Novel donepezil-based inhibitors of acetyl- and butyrylcholinesterase and acetylcholinesterase-induced beta-amyloid aggregation. *J. Med. Chem. 51*, 3588−3598.
(25) Rodríguez-Franco, M. I., Fernández-Bachiller, M. I., Pérez, C., Hernández-Ledesma, B., and Bartolomé, B. (2006) Novel tacrine-melatonin hybrids as dual-acting drugs for Alzheimer disease, with improved acetylcholinesterase inhibitory and antioxidant properties. *J. Med. Chem. 49*, 459−462.
(26) Fang, L., Kraus, B., Lehmann, J., Heilmann, J., Zhang, Y., and Deckera, M. (2008) Design and synthesis of tacrine-ferulic acid hybrids as multi-potent anti-Alzheimer drug candidates. *Bioorg. Med. Chem. Lett. 18*, 2905−2909.
(27) Sheng, R., Xu, Y., Hu, C., Zhang, J., Lin, X., Li, J., Yang, B., He, Q., and Hu, Y. (2009) Design, synthesis and AChE inhibitory activity of indanone and aurone derivatives. *Eur. J. Med. Chem. 44*, 7−17.
(28) Piazzi, L., Cavalli, A., Colizzi, F., Belluti, F., Bartolini, M., Mancini, F., Recanatini, M., Andrisano, V., and Rampa, A. (2008) Multi-target-directed coumarin derivatives: hAChE and BACE1 inhibitors as potential anti-Alzheimer compounds. *Bioorg. Med. Chem. Lett. 18*, 423−426.
(29) Mattson, M. P., and S. L. Chan, S. L. (2001) Dysregulation of cellular calcium homeostasis in Alzheimer's disease: bad genes and bad habits. *J. Mol. Neurosci. 17*, 205−224.
(30) Hölscher, C. (1998) Possible causes of Alzheimer's disease: amyloid fragments, free radicals, and calcium homeostasis. *Neurobiol. Dis. 5*, 129−141.
(31) Ripová, D., Platilová, V., Struneká, A., Jirák, R., and Höschl, C. (2000) Cytosolic calcium alterations in platelets of patients with early stages of Alzheimeŕs disease. *Neurobiol. Aging 5*, 729−734.
(32) Demuro, A., Parker, I., and Stutzmann, G. E. (2010) Calcium signaling and amyloid toxicity in Alzheimer disease. *J. Biol. Chem. 285*, 112463−12468.
(33) Bezprozvanny, I., and Mattson, M. P. (2008) Neuronal calcium mishandling and the pathogenesis of Alzheimer's disease. *Trends Neurosci. 31*, 454−463.
(34) Mattson, M. P. (2007) Calcium and neurodegeneration. *Aging Cell 6*, 337−350.
(35) Léon, R., and Marco-Contelles, J. (2011) A step further towards multitarget drugs for Alzheimer and neuronal vascular diseases: Targeting the cholinergic system, amyloid-$\beta$ aggregation and $Ca^{2+}$ dyshomeostasis. *Curr. Med. Chem. 18*, 552−576.
(36) León, R., García, A. G., and Marco-Contelles, J. (2013) Recent advances in the multitarget-directed ligands approach for the treatment of Alzheimer's Disease. *Med. Res. Rev. 33*, 139−189.
(37) Alonso, D., Dorronsoro, I., Rubio, L., Muñoz, P., García-Palomero, E., del Monte, M., Bidon-Chanal, A., Orozco, M., Luque, F. J., Castro, A., Medina, M., and Martínez, A. (2005) Donepezil-tacrine hybrid related derivatives as new dual binding site inhibitors of AChE. *Bioorg. Med. Chem. 13*, 6588−6597.
(38) Samadi, A., Marco-Contelles, J., Soriano, E., Álvarez-Pérez, M., Chioua, M., Romero, A., González-Lafuente, L., Gandía, L., Roda, J. M., López, M. G., Villarroya, M., García, A. G., and de los Ríos, C. (2010) Multipotent drugs with cholinergic and neuroprotective properties for the treatment of Alzheimer and neuronal vascular diseases. I. Synthesis, biological assessment, and molecular modeling of simple and readily available 2-aminopyridine-, and 2-chloropyridine-3,5-dicarbonitriles. *Bioorg. Med. Chem. 18*, 5861−5872.
(39) Scipione, L., De Vita, D., Musella, A., Flammini, L., Bertoni, S., and Barocelli, E. (2008) 4-Aminopyridine derivatives with anti-cholinesterase and antiamnesic activity. *Bioorg. Med. Chem. Lett. 18*, 309−312.
(40) Very surprisingly, compounds **12** and **13** proved good and selective inhibitors of *Ee*AChE, showing $IC_{50}$ 6.0 ± 0.5 and 2.1 ± 0.5 $\mu$M, respectively. This unexpected result has prompted us to investigate in depth this family of simple and readily available AChE inhibitors. Results are in progress, and will be reported elsewhere in due course.
(41) Elkasaby, M. A., and F. Elshahed, F. (1981) Synthesis and reactions of 4-aryl-5-carbethoxy-3-cyano-6-methyl-2(H)-pyridones. *Indian J. Chem., Sect. B: Org. Chem. Incl. Med. Chem. 20B*, 428−431.
(42) Contreras, J. M., Rival, Y. M., Chayer, S., Bourguignon, J. J., and Wermuth, C. G. (1999) Aminopyridazines as acetylcholinesterase inhibitors. *J. Med. Chem. 42*, 730−741.
(43) Samadi, A., Chioua, M., Bolea, I., de los Ríos, C., Iriepa, I., Moraleda, I., Bastida, A., Esteban, G., Unzeta, M., Gálvez, E., and

Marco-Contelles, J. (2011) Synthesis, biological assessment and molecular modeling of new, multipotent MAO and cholinesterase inhibitors as potential drugs for the treatment oif Alzheimeŕs disease. *Eur. J. Med. Chem. 46*, 4665−4668.
(44) Bolea, I., Juárez, J., de los Ríos, C., Chioua, M., Pouplana, R., Luque, F. J., Unzeta, M., Marco-Contelles, J., and Samadi, A. (2011) Synthesis, biological evaluation, and molecular modeling of donepezil and *N*-[(5-(benzyloxy)-1-methyl-1H-indol-2-yl)methyl]-*N*-methyl-prop-2-yn-1-amine hybrids as new multipotent cholinesterase/monoamine oxidase inhibitors for the treatment of Alzheimer's disease. *J. Med. Chem. 54*, 8251−8270.
(45) Marco-Contelles, J., Pérez-Mayoral, M. E., Samadi, A., Carreiras, M. C., and Soriano, E. (2009) Recent Advances in the Friedländer reaction. *Chem. Rev. 109*, 2652−2671.
(46) Marco, J. L., and Carreiras, M. C. (2010) *The Friedländer Reaction*, LAP Lambert Academic Publishing AG & Co. KG, Saarbrücken, Germany.
(47) Fernandez-Mato, A., Blanco, G., Quintela, J. M., and Peinador, C. (2008) Synthesis of new bis(2.[1,8]naphthyridinyl) bridging ligands with multidentate binding sites. *Tetrahedron 64*, 3446−3456.
(48) Nagarajan, S., and Das, T. M. (2009) Facile one-pot synthesis of sugar-quinoline derivatives. *Carbohydr. Res. 344*, 1028−1031.
(49) Dormer, P. G., Eng, K. K., Farr, R. N., Humphrey, G. R., McWilliams, J. C., Reider, P. J., Sager, J. W., and Volante, R. P. (2003) Highly regiosselective Friedländer annulations with unmodified ketones employing novel amine catalysts: Syntheses of 2-substituted quinolines, 1,8-naphthyridines, and related heterocycles. *J. Org. Chem. 68*, 467−477.
(50) Silva, D., Chioua, M., Samadi, A., Carreiras, M. C., Jimeno, M.-L., Mendes, M. E., de los Ríos, C., Romero, A., Villarroya, M., López, M. G., and Marco-Contelles, J. (2011) Synthesis and pharmacological assessment of diversely substituted pyrazolo[3,4-*b*]quinoline, and benzo[*b*]pyrazolo[4,3-*g*][1,8]naphthyridine derivatives. *Eur. J. Med. Chem. 46*, 4676−4681.
(51) Ellman, G. L., Courtney, K. D., Andres, V., Jr., and Feather-Stone, R. M. (1961) A new and rapid colorimetric determination of acetylcholinesterase activity. *Biochem. Pharmacol. 7*, 88−95.
(52) Greig, N. H., Utsuki, T., Ingram, D., Wang, K. Y., Pepeu, G., Scali, C., Yu, Q. S., Mamczarz, J., Holloway, H. W., Giordano, T., Chen, D., Furukawa, K., Sambamurti, K., Brossi, A., and Lahiri, D. K. (2005) Selective butyrylcholinesterase inhibition elevates brain acetylcholine, augments learning and lowers Alzheimer beta-amyloid peptide in rodent. *Proc. Natl. Acad. Sci. U.S.A. 102*, 17213−17218.
(53) Chan, S. L., Shirachi, D. Y., Bhargava, H. N., Gardner, E., and Trevor, A. J. (1972) Purification and properties of multiple forms of brain acetylcholinesterase (EC 3.1.1.7). *J. Neurochem. 19*, 2747−58.
(54) Ott, P., Lustig, A., Brodbeck, U., and Rosenbusch, J. P. (1982) Acetylcholinesterase from human erythrocytes membranes: dimers as functional units. *FEBS Lett. 138*, 187−189.
(55) Rosenberry, T. L., Mallender, W. D., Thomas, P. J., and Szegletes, T. (1999) A steric blockade model for inhibition of acetylcholinesterase by peripheral site ligands and substrate. *Chem.-Biol. Interact. 119−120*, 85−97.
(56) Lopes, J. P., Oliveira, C. R., and Agostinho, P. (2009) Cdk5 acts as a mediator of neuronal cell cycle re-entry triggered by amyloid-beta and prion peptides. *Cell Cycle 8*, 97−104.
(57) Melo, J. B., Agostinho, P., and Oliveira, C. R. (2003) Involvement of oxidative stress in the enhancement of acetylcholinesterase activity induced by amyloid beta-peptide. *Neurosci. Res. 45*, 117−27.
(58) Thullbery, M. D., Cox, H. D., T. Schule, T., Thompson, C. M., and George, K. M. (2005) Differential localization of acetylcholinesterase in neuronal and non-neuronal cells. *J. Cell Biochem. 96*, 599−610.
(59) Dajas-Bailador, F. A., Heimala, K., and Wonnacott, S. (2003) The allostreric potentiation of nicotinic acetylcholine receptors by galantamine is transduced into cellular responses in neurons: $Ca^{2+}$ signals and neurotransmitter release. *Mol. Pharmacol. 64*, 1217−1226.
(60) Solntseva, E. I., Bukanova, J. V., Marchenko, E., and Skrebitsky, V. G. (2007) Donepezil is a strong antagonist of voltage-gated calcium and potassium channels in molluscan neurons. *Comp. Biochem. Physiol., Part C: Toxicol. Pharmacol. 144*, 319−326.
(61) Trott, O., and Olson, A. J. (2010) AutoDockVina: improving the speed and accuracy of docking with a new scoring function, efficient optimization and multithreading. *J. Comput. Chem. 31*, 455−461.
(62) Bartolini, M., Pistolozzi, M., Andrisano, V., Egea, J., López, M. G., Iriepa, I., Moraleda, I., Gálvez, E., Marco-Contelles, J., and Samadi, A. (2011) Chemical and pharmacological studies on enantiomerically pure p-methoxytacripyrines, promising multi-target-directed ligands for the treatment of Alzheimer's disease. *ChemMedChem 6*, 1990−1997.
(63) Martins, C., Carreiras, M. C., Leon, R., de los Rios, C., Bartolini, M., Andrisano, V., Iriepa, I., Moraleda, I., Galvez, E., Garcia, M., Egea, J., Samadi, A., Chioua, M., and Marco-Contelles, J. (2011) Synthesis and biological assessment of diversely substituted furo[2,3-b]quinolin-4-amine and pyrrolo[2,3-b]quinolin-4-amine derivatives, as novel tacrine analogues. *Eur. J. Med. Chem. 46*, 6119−6130.
(64) Samadi, A., de los Rios, C., Bolea, I., Chioua, M., Iriepa, I., Moraleda, I., Bartolini, M., Andrisano, V., Galvez, E., Valderas, C., Unzeta, M., and Marco-Contelles, J. (2012) Multipotent MAO and cholinesterase inhibitors for the treatment of Alzheimer's disease: Synthesis, pharmacological analysis and molecular modeling of heterocyclic substituted alkyl and cycloalkyl propargyl amine. *Eur. J. Med. Chem. 52*, 251−262.
(65) Maalej, E., Chabchoub, F., Oset-Gasque, M. J., Esquivias-Pérez, M., González, M. P., Monjas, L., Pérez, C., de los Ríos, C., Rodríguez-Franco, I., Iriepa, I., Moraleda, I., Chioua, M., Romero, A., Marco-Contelles, J., and Samadi, A. (2012) Synthesis, biological assessment, and molecular modeling of racemic 7-aryl-9,10,11,12-tetrahydro-7H-benzo[7,8]chromeno[2,3-b]quinolin-8-amines as potential drugs for the treatment of Alzheimer's disease. *Eur. J. Med. Chem. 54*, 750−763.
(66) Wallace, A. C., Laskowski, R. A., and Thornton, J. M. (1996) LIGPLOT: a program to generate schematic diagrams of protein-ligand interactions. *Protein Eng. 8*, 127−134.
(67) Arnold, K., Bordoli, L., Kopp, J., and Schwedge, T. (2006) The SWISS-MODEL Workspace: A web-based environment for protein structure homology modelling. *Bioinformatics 22*, 195−201.
(68) Kiefer, F., Arnold, K., Künzli, M., Bordoli, L., and Schwede, T. (2009) The SWISS-MODEL Repository and associated resources. *Nucleic Acids Res. 37*, D387−D392.
(69) Peitsch, M. C. (1995) Protein modeling by E-mail. *Bio/Technology 13*, 658−660.
(70) Eichler, J., Anselment, A., Sussman, J. L., Massoulié, J., and Silman, J. (1994) Differential effects of "peripheral" site ligands on Torpedo and chicken acetylcholinesterase. *Mol. Pharmacol. 45*, 335−40.
(71) Resende, R., Ferreiro, E., Pereira, C., and Oliveira, C. R. (2008) Neurotoxic effect of oligomeric and fibrillar species of amyloid-beta peptide 1−42: Involvement of endoplasmic reticulum calcium release in oligomer-induced cell death. *Neuroscience 155*, 725−737.
(72) Brooks, B. R., Bruccoleri, R. E., Olafson, B. D., States, D. J., Swaminathan, S., and Karplus, M. (1983) Charmm, a program for macromolecular energy, minimization, and dynamics calculations. *J. Comput. Chem. 4*, 187−217.
(73) Morreale, A., Maseras, F., Iriepa, I., and Gálvez, E. (2002) Ligand-receptor interaction at the neural nicotinic acetylcholine binding site: A theoretical model. *J. Mol. Graphics Modell. 21*, 111−118.